2014

Turbulence convective heat transfer for cooling the photovoltaic cells

Iman Arianmehr
University of Windsor

TURBULENCE CONVECTIVE HEAT TRANSFER FOR COOLING THE PHOTOVOLTAIC CELLS

By

Iman Arianmehr

A Thesis
Submitted to the Faculty of Graduate Studies
through the Department of Mechanical, Automotive and Material Engineering
in Partial Fulfillment of the Requirements for
the Degree of Master of Science
at the University of Windsor

Windsor, Ontario, Canada

2014

Turbulence Convective Heat Transfer For Cooling the Photovoltaic Cells

by

Iman Arianmehr

APPROVED BY:

_____

P. Henshaw
Department of Civil and Environmental Engineering

_____

A. Fartaj
Department of Mechanical, Automotive and Material Engineering

_____

S. Ray, Industrial Adviser
Essex Energy

_____

D. S-K. Ting, Adviser
Department of Mechanical, Automotive and Material Engineering

16 April 2014

DECLARATION OF ORIGINALITY

I. Declaration of Previous Publication

This thesis includes three original papers that have been previously published/submitted for publication in peer reviewed journals, as follows:

Thesis Chapter	Publication Title	Publication Status
Chapter 2	Assisted Turbulence Convection Heat Transfer for Cooling the Photovoltaic Cells, I. Arianmehr, D.S-K. Ting , S. Ray, Proceedings of the ASME 2013 Summer Heat Transfer Conference, HT2013-17210, pp. V001T01A028; 10 pages, doi:10.1115/HT2013-17210	Proceedings of the ASME 2013 Summer Heat Transfer Conference
Chapter 3	An Experimental Investigation on Passive Cooling of a Surrogate Photovoltaic Panel, I. Arianmehr, D.S-K. Ting , S. Ray	For submission to: Journal of Solar Energy Engineering, under review
Chapter 4	Convective Cooling of a Surrogate Photovoltaic Panel with a Transverse Groove, I. Arianmehr, D.S-K. Ting , S. Ray	For submission to: ASME 2014 International Mechanical Engineering Congress & Exposition

I certify that I have obtained a written permission from the copyright owner(s) to include the above published material(s) in my thesis. I certify that the above material describes work completed during my registration as graduate student at the University of Windsor.

I declare that, to the best of my knowledge, my thesis does not infringe upon anyone's copyright nor violate any proprietary rights and that any ideas, techniques, quotations, or any other material from the work of other people included in my thesis, published or otherwise, are fully acknowledged in accordance with the standard referencing practices.

Furthermore, to the extent that I have included copyrighted material that surpasses the bounds of fair dealing within the meaning of the Canada Copyright Act, I certify that I have obtained a written permission from the copyright owner(s) to include such material(s) in my thesis.

I declare that this is a true copy of my thesis, including any final revisions, as approved by my thesis committee and the Graduate Studies office, and that this thesis has not been submitted for a higher degree to any other University or Institution.

ABSTRACT

Solar PV (photovoltaic) is a rapidly advancing renewable energy technology which converts sunlight directly into electricity. One of the outstanding challenges of the current PV technology is the reduction in its conversion efficiency with increasing PV panel temperature, which is closely associated with the increase in solar intensity and the ambient temperature surrounding the PV panels. To more effectively capture the available energy when the sun is most intense, significant efforts have been invested in active and passive cooling research over the last few years. While integrated cooling systems can lead to the highest total efficiencies, they are usually neither the most feasible nor the most cost effective solutions. This work examines some simple passive means of manipulating the prevailing wind turbulence to enhance convective heat transfer over a heated plate in a wind tunnel.

DEDICATION

This work is dedicated to my wife whose love, loyalty and resourcefulness I will forever be indebted to and to my parents to whom I give credit for all that has been accomplished.

ACKNOWLEDGEMENTS

Foremost, I would like to express my profound gratitude to my primary advisor Dr. Ting and my industrial advisor Mr. Ray for their patience and continuous support. Their guidance helped me greatly throughout this thesis.

I would also like to acknowledge the financial support from the Natural Sciences and Engineering Research Council of Canada. This is a project cosponsored by Ontario Centres of Excellence and Essex Energy Corporation.

My sincere acknowledgment also goes for the staff of University of Windsor, especially Mr. A. Jenner and Mr. P. Seguin, for their technical assistant.

Last but not the least; I owe my loving thanks to my wife. Without her encouragement and support it would not have been possible for me to finish this work.

TABLE OF CONTENTS

LIST OF TABLES

Chapter 2

Chapter 3

Chapter 4

LIST OF FIGURES

Chapter 2

Chapter 3

Chapter 4

Appendix A

CHAPTER 1

INTRODUCTION

Solar energy is one of the most important renewable energy sources, since it provides unlimited, clean, and environmentally friendly energy [1]. One of the most considerable and fast-growing applications of sunlight is conversion of solar radiation directly to the electricity by PV (photovoltaic) cells. Intensive efforts are being made to improve efficiency of PV cells and decrease the cost per peak power gained from them. Besides the improvement of the production techniques and new materials, providing an effective operating condition can be important. In the present commercial PV cell, however, only a fraction of absorbed sunlight is converted into electricity. The efficiency of a typical PV cell is less than twenty percent [2]. The remainder of the absorbed energy will be converted into the heat energy in the cell and can cause the cell's temperature to rise. The effect of temperature on the performance of PV cells was reported in [3] and [4]. It is well known that the efficiency of a PV cell decreases with increasing cell temperature. With a temperature increase of 1°C above 25°C for a crystalline solar cell, the output power of the cell can decrease by 0.4% [5], [6]. This reduction is about 0.25% for amorphous silicon cells [7]. Therefore, it is necessary to dissipate heat generated to the ambient and keep cell temperature as low as possible.

PV-Thermal (PVT) systems combine a photovoltaic cell, which converts electromagnetic radiation (photons) into electricity, with a solar thermal collector, which captures the remaining energy and removes waste heat from the PV module. Such systems can be engineered to carry heat away from the PV cells, thereby cooling the cells and thus improving their efficiency. A PVT module according to its application can employ air or liquid as the coolant. A liquid PVT collector is similar to a conventional flat plate collector whose absorber is covered by a suitable PV layer [8]. The thermal energy is distributed to a fluid, whereas the PV layer produces electricity [9]. The final result of this arrangement is the combined production of the electricity and heat, including growing the efficiency of the PV cell by spreading the heat out of it. When the operating temperature raises, the power decreases. So, the outlet temperature of the cooling fluid should be sufficiently low (usually <40°C) [10]. For this reason the heat produced from a PVT system can be used only in cases when low temperature heat is in demand, such as domestic hot water production, floor heating, and desiccant cooling [11]. The most common PVT air configuration consists of an air duct directly beneath a photovoltaic array; however a number of different designs for PVT air collectors have been explored through experimentation and analytical analysis and presented in the literature. In the mentioned methods, external power is required for flowing coolant. So, pumping can consume some part of generated output power of PV cells. It is one of the considerations in cooling system design. However, active cooling systems can be cost effective, if the extracted thermal energy form the PV cells used in the heating system is taken into consideration. Wind-induced convective heat transfer can be used for cooling of the PV

cell without an external pump driving force. Developing a passive cooling method of PV panels by enhancing the wind-induced convective heat transfer can increase the conversion efficiency of PV cells. External power is not required in this method; simplicity, as well as a reduction in the initial, operational, and maintenance costs is promised. In addition, the design of devices that promote passive cooling methods may be easy to retrofit onto the fixtures of existing PV modules. The following publications are the results of research on a passive cooling method for improving the efficiency of photovoltaic panels.

Chapter 2 of this work examines some simple passive means of manipulating the prevailing wind turbulence to enhance convective heat transfer over a heated plate in a wind tunnel. Specific turbulence generators are devised based on knowledge gained from an orifice perforated plate turbulence study. Temperature and heat flux of the plate were measured. Then the effects of the orifice perforated plate on the temperature distribution and heat transfer were studied. In order to better understand the effect of an orifice perforated plate on the effectiveness of the local heat transfer, the characteristics of the flow were studied and the results have been presented in Chapter 3. The effect of a transverse rectangular groove on cooling of the PV panel (heated flat plate) has been studied in Chapter 4. A simple rectangular groove of variable width was machined near the leading edge of the heated plate. This simple surface roughening was chosen over an array of riblets because of ease of fabrication, limited space and maintenance of the structural integrity of the PV panel / frame. Despite the fact that a wide range of grooves has been studied over the years, there is still a lack of consensus concerning this effect on the resulting flow and heat transfer characteristics. Chapter 5 provides some recommendations for further research in order to improve cooling of the photovoltaic panel.

REFERENCES

[1] Luque A., Hegedus S. Handbook of Photovoltaic Science and Engineering. 2nd Ed., Wiley, 2011.

[2] Huang B.J., Lin T.H., Hung W.C., Sun F.S. Performance evaluation of solar photovoltaic/thermal systems. Solar Energy, 70(5): 443–448, 2001.

[3] Radziemska E. The effect of temperature on the power drop in crystalline silicon solar cells. Renewable Energy, 28: 1–12, 2003.

[4] Vorobiev Y.V., Gorley N. Photovoltaic solar cells performance at elevated temperatures. Solar Energy, 78: 243–50, 2005.

[5] Hausler T., Rogass H. Latent heat storage on photovoltaic. Sixteenth European Photovoltaic Solar Energy Conference, Glasgow, UK, 2265–2267, 2000.

[6] Brinkworth B.J., Cross B.M., Marshall R.H., Yang H. Thermal regulation of photovoltaic cladding. Solar Energy, 61(3): 169–178, 1997.

[7] Kalogirou S.A., Tripanagnostopoulos Y. Hybrid PV/T solar systems for domestic hot water and electricity production. Energy Conversion Management, 47: 3368–3382, 2006.

[8] Zondag H.A. Flat-plate PV-thermal collectors and systems: a review, Renewable Sustainable Energy Review, 12: 891–895, 2008.

[9] Chow T.T. Photovoltaic/thermal hybrid solar technology: a review, Applied Energy, 87: 365–379, 2010.

[10] Skoplaki E., Palyvos J.A. On the temperature dependence of photovoltaic module electrical performance: a review of efficiency/power correlations Solar Energy, 83: 614–624, 2009.

[11] Beccali M., Finocchiaro P., Nocke B., Energy and economic assessment of desiccant cooling systems coupled with single glazed air and hybrid PV/thermal solar collectors for applications in hot and humid climate, Solar Energy, 83: 1828–1846, 2009.

CHAPTER 2

ASSISTED TURBULENCE CONVECTIVE HEAT TRANSFER FOR COOLING PHOTOVOLTAIC CELLS

I. ARIANMEHR, D.S-K. TING* , S. RAY, PROCEEDINGS OF THE ASME 2013 SUMMER HEAT TRANSFER CONFERENCE, HT2013-17210, PP. V001T01A028; 10 PAGES, DOI:10.1115/HT2013-17210

1. ABSTRACT

Solar PV (photovoltaic) is a rapidly advancing renewable energy technology which converts sunlight directly into electricity. One of the outstanding challenges of the current PV technology is the reduction in its conversion efficiency with increasing PV panel temperature, which is closely associated with the increase in solar intensity and the ambient temperature surrounding the PV panels. To more effectively capture the available energy when the sun is most intense, significant efforts have been invested in active and passive cooling research over the last few years. While integrated cooling systems can lead to the highest total efficiencies, they are usually neither the most feasible nor the most cost effective solution. This work examines some simple passive means of manipulating the prevailing wind to enhance convective heat transfer over a heated plate in a wind tunnel. Specific turbulence generators are devised based on knowledge gained from an orificed perforated plate turbulence study.

NOMENCLATURE

h_x	Local Heat Transfer Coefficient ($W/m^2°C$)
k	Thermal Conductivity (W/m·°C)
N	Normalized Local Nusselt Number
Nu_x	Local Nusselt Number
q	Heat Flux Rate (W/m^2)
Re_x	Local Reynolds Number
T_f	Film Temperature (°C)
T_s	Measured Surface Temperature (°C)
T_∞	Free Stream Temperature (°C)
x	Distance From The Leading Edge (cm)

* Corresponding Author: dting@uwindsor.ca

Greek Symbols

ϑ	Kinematic Viscosity (m^2/s)

Subscripts

cr	Critical
f	Film
s	Surface
x	Local
∞	Free Stream

2. INTRODUCTION

Solar is a promising renewable energy source for producing clean and environmentally friendly energy [1]. One of the fastest-growing applications of the sunlight is the direct conversion of solar radiation into electricity via PV (photovoltaic) cells. Intensive efforts are ever being made to further the efficiency of PV cells and to decrease the associated manufacturing costs. Besides the progress in the manufacturing techniques and the improvement of the materials, optimizing the operating conditions of the actual energy conversion process is equally important.

At present, the best non-concentrator mono crystalline silicon cells have a laboratory operating efficiency of around 25% [2], while concentrator multi-junction cells have a demonstrated efficiency as high as 44% in a well-controlled laboratory environment [2]. Typical mass-produced commercial mono-crystalline PV cells have an efficiency of less than 22.5% in the field [3]. Thus, only a fraction of the absorbed sunlight is converted into electricity in real applications. The remainder of the absorbed energy becomes waste heat, which can cause the temperature of the cells to rise, and consequently, lower the conversion efficiency [4,5]. Under direct sunshine the nominal operating temperature of PV cells can reach 33-55°C [6]. Therefore, it is beneficial to dissipate the heat generated into the ambient, thus keeping the cells cool so as to maintain high energy conversion efficiency and to lower thermal stresses.

3. COOLING METHODS

Some existing methods of cooling the PV cells are briefly reviewed here. First of all there is the PV-Thermal (PVT) system which is a hybrid of solar PV and solar thermal. These systems combine photovoltaic cells, which convert electromagnetic radiation (photons) into electricity, with a solar thermal collector, which captures the remaining energy and removes the waste heat from the PV module. Both air and liquid (water) can be employed as the coolant for these PVT systems. The liquid PVT collectors, as shown in

Fig. 2.1, are similar to a conventional flat plate collector, except the absorber is covered by an appropriate PV layer [7]. The system aims at maximizing the conversion of the available solar energy into electricity via the PV layer, with the un-captured thermal energy distributed into the flowing coolant [8]. As such, the thermal energy collection also ensures some amount of PV layer cooling. To maintain a minimum level of performance, the outlet temperature of the coolant should be sufficiently low (usually <40°C) [9]. For this reason the heat produced from PVT systems can be used only in low temperature heat application, such as domestic hot water production, floor heating, and desiccant cooling [10].

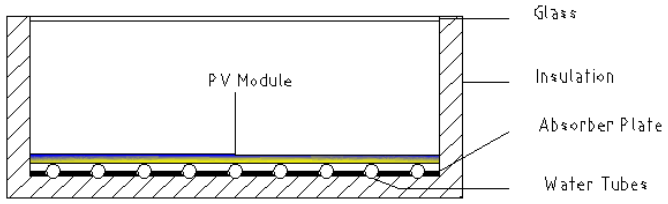

(a) Glazed

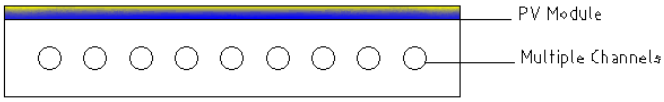

(b) Unglazed

Figure 2.1: Cross-section of a basic liquid PVT collector.

The most common PVT air consists of an air duct directly beneath a photovoltaic array; however, there are other designs of PVT air collectors which have been explored and documented in the literature. Performance improvements of an air cooled PVT collector using a suspended metal sheet at the middle of the air channel have been investigated by Tonui and Tripanagnostopoulos [11]. Relationships between heat output and temperature rise of various PVT designs have been studied by Bambrook and Sproul [12]. In order to enhance heat transfer from the PV module, Prasad and Saini [13] artificially increased the roughness of the absorber plate and walls of the channel. Increasing roughness, however, leads to increased pressure drop, and thus, increased pumping power. De Vries [14] proposed a dual-flow PVT-collector with a reversed water flow (water inlet above the PV, water exit below the PV), with an insulating air layer between PV and the lower channel. Kumar and Rosen [6] evaluated the performance of a double pass PV/T solar air heater with and without fins; the cross section of their proposed system is shown in Fig. 2.2. The extended surface on the absorber reduced the module temperature and increased the performance of the cells. Tao et al. [15] experimentally and numerically showed that by a duct flow fabricated at the back of the

PV module with fins fitted in the duct the electrical efficiency of PV cell can increase from 8.6% to 12.5%. Although PVT technology is still relatively new, it has, nonetheless, navigated its way into practical applications. For instance, the Canadian company 'Conserval Engineering Inc' provides the rooftop SolarDuct and SolarWall products [16]. SolarWall is a PVT system that can heat up air for domestic, agricultural and manufacturing applications [17]. It can produce up to 400% more usable energy than a solely photovoltaic system. The SolarDuct PVT (Fig. 2.3) is a rooftop module with a combined electrical and thermal efficiency of more than 50% [18]. Another appropriate technique for PV cooling is by using water flow over the upper surface of a PV cell. This technique was used in a PV façade, and an increase in output electric power of 10.3% has been reported [19].

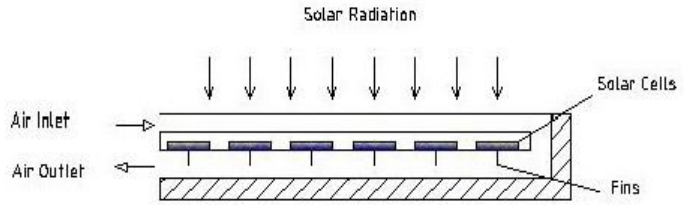

Figure 2.2: Cross-sectional view of double-pass PV/T solar air heater with fins [6].

In the aforementioned methods, some amount of electric power is required to move the coolant. In other words, a portion of the harvested power is used to run the system, and hence lowering the overall efficiency accordingly. Minimizing the needed pumping power is one of the challenges in any cooling system design. Passive cooling of PV panels by enhancing the wind induced convective heat transfer does not require power consumption, and it promises significant simplicity, lowering the initial, operational and maintenance costs. These passive devices can be designed such that they can be easily mounted onto the fixtures of existing PV panels.

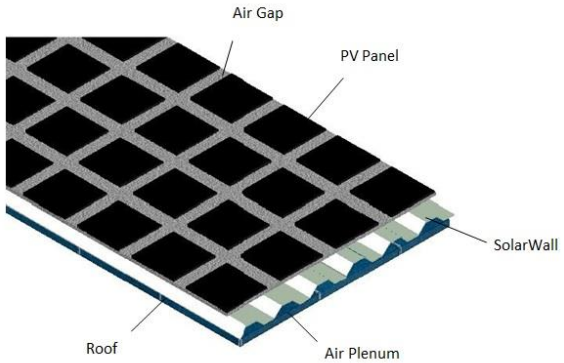

Figure 2.3: The solar air PV/T products of 'Conserval Engineering' company [17].

Wind induced convection heat transfer has been evaluated by many researchers. Karava et al. [20] investigated the effect of incident flow conditions on forced convective heat transfer from an integrated PV/T system on an inclined roof. The efficiency of a corrugated unglazed transpired solar collector combined with a photovoltaic system has been studied by Bambadra [21]. The results show that the overall efficiency of system can be up to 70%. Selecting the most appropriate available wind-convection heat transfer correlations in the literature for a particular application depends on parameters including the characteristic lengths, wind speed, wind turbulence, wind direction, etc under consideration. Some of the available data are based on wind tunnel studies for relatively small plates [22-24], while others are acquired in full scale field with actual buildings [25-29]. Furthermore, there have been attempts such as that made by Palyvos [30], try putting the wide range of results into perspective.

4. EXPERIMENTAL SETUP

The experiments were conducted in a closed loop wind tunnel. The test section is roughly 762×762 mm with a length of 1.8 m. The velocity profile was deduced based on 15×50 (horizontally and vertically as illustrated in Fig. 2.4) hot-wire measurements. This was performed by traversing the hot-wire probe over the 750 grid points at the leading edge of model solar panel (a heated flat plate) in the absence of the model. The air velocity was quantified using a Dantec constant temperature anemometer (CTA) module 90C10 with a Dantec Type 55P11 miniature wire straight probe. It has 5 µm diameter and 1.25 mm long platinum-plated tungsten wire sensors. The analog voltage signals were first low-passed at 30 kHz using an analog filter to avoid aliasing and were sampled at 80 kHz over a 25 s period (2,000,000 samples) through a 12-bit PCI-6071E National Instrument data acquisition card.

The velocity in the Z (flow stream) direction is plotted as a function of the X-Y coordinate in Fig. 2.5. It is clear that the velocity profile for the entire cross section outside the boundary layer is reasonably flat. The boundary layer thickness can be estimated from the velocity profiles. It is the point where the velocity drops below 95% of the nominal free stream value; and approaches to zero near the wind tunnel walls. It is less than 15 mm, the first measurement point from the wall. A typical set of local time averaged velocity values and their standard deviations are plotted in Fig. 2.6. It can be seen that the maximum standard deviation is less than 5.4%.

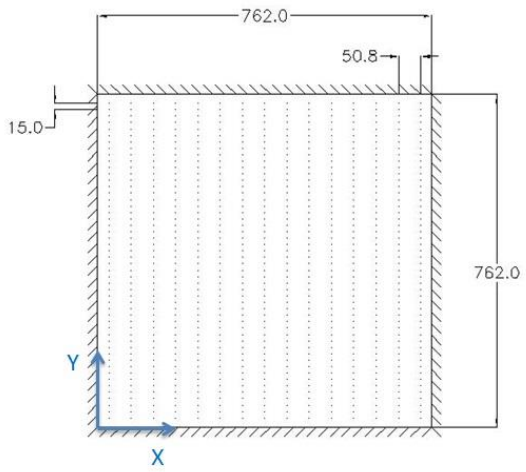

Figure 2.4: Cross section of the test section – dimensions and arrangement of the measurement grid (dimensions are in millimeter).

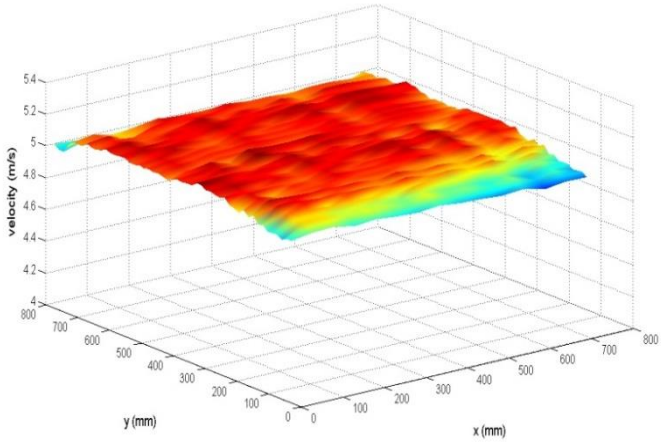

Figure 2.5: Air velocity profile at the test inlet section (15×50 grid point measurement, upstream air velocity measured by manometer is 5.02 m/s , with turbulent intensity of Tu=0.2%).

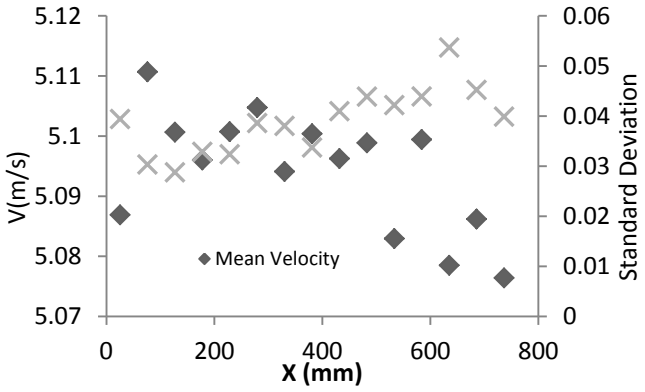

Figure 2.6: Mean value of air velocity and standard deviations in every column measured by hot-wire.

The solar panel was surrogated by a 522 mm by 337 mm aluminum flat plate equipped with a 457.2 ×304.8 mm silicone-rubber heating pad for easy control of the surface temperature. Fig. 2.7 depicts the energy balance of the heated plate. At steady state condition, the input energy to the plate (Q_0) is equal to the energy which is transferred from the flat plate to the free stream via convection (Q_{conv}), conduction (Q_{cond}) and radiation (Q_{rad}) heat transfer. Carbon fiber and particle board layers (see Fig. 2.8) were employed to insulate the bottom from the surrounding and hence, reduce heat loss from the back of the plate.

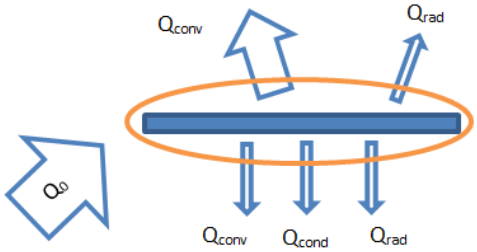

Figure 2.7: Energy balance under steady state condition.

Figure 2.8: Fiber carbon left, silicon rubber heater right.

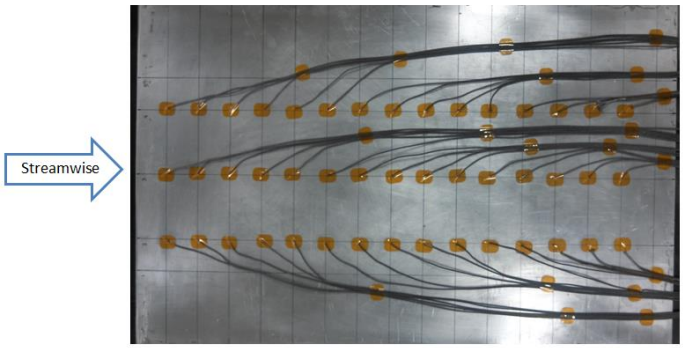

Figure 2.9: Thermocouples arrangement.

The surface temperature distribution was monitored by 45 type T thermocouples mounted on the back of the aluminum sheet as shown in Fig. 2.9. Thermocouple adhesive pads were used to secure wire probes to surface. The distances between two consecutive rows or columns are 3 and 6 cm, respectively. This particular distribution aims at maximizing the coverage over the area of interest. The local heat flux was measured by a heat transfer sensor manufactured by Hukseflux, model PU-11, which has an accuracy of ±5% of the reading.

The complete experimental setup is shown in Fig. 2.10. A turbulence generator as detailed in Fig. 2.11 was employed, aiming to significantly enhance the incoming wind turbulence. It was attached to the leading edge of the heated plate setup as portrayed in Figs. 2.10 and 2.12. The heated plate was placed at half height and in the middle of the test section. The free stream velocity in the wind tunnel was monitored by a Pitot-static tube, which was connected to a digital manometer (Dwyer series 475 mark II).

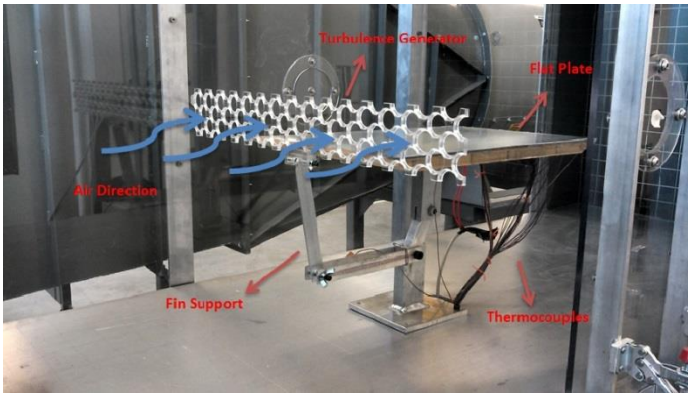

Figure 2.10: Experimental setup in the wind tunnel.

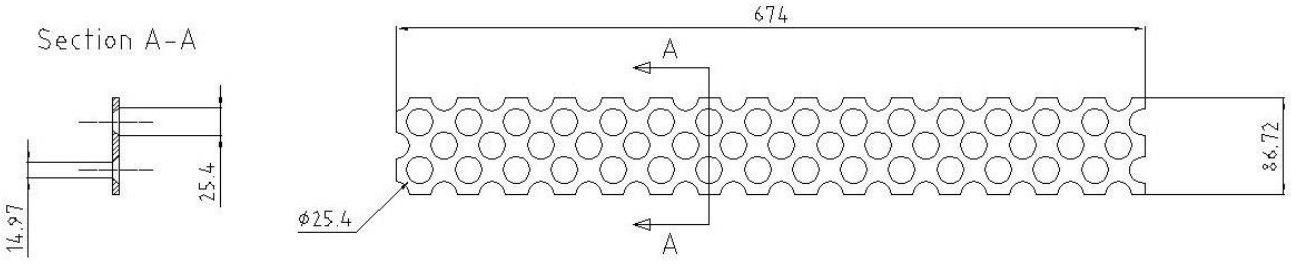

Figure 2.11: Geometry of turbulence generator (dimensions are in mm).

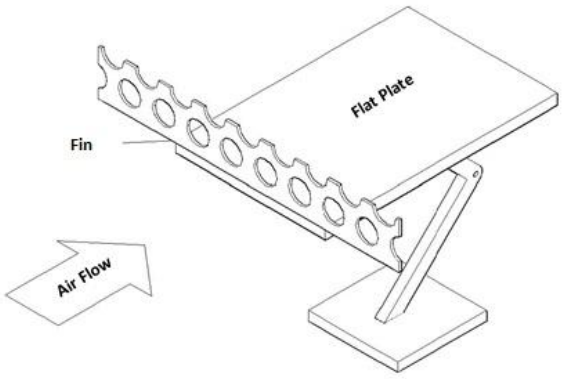

Figure 2.12: Isometric drawing of turbulence generator (fin) on the leading edge of the flat plate.

5. RESULTS AND DISCUSSION

First, the experiments were carried out for the flat plate without the turbulence generator (fin). Then the effects of the fin on the temperature distribution and heat transfer were studied. After turning the heater and the wind tunnel on, it took about two hours for the system to reach thermal equilibrium. With the system operating under steady state condition, five repeated temperature measurements were conducted at 15 minute intervals, and the resulting data were used to provide the local mean temperature and local heat flux distribution along the heated plate. The experiments were carried out for mean wind speeds of 2.68, 4.12, 5.02, and 6.16 m/s. The temperature contours of the middle 6 cm width and 45 cm long section of the heated plate, in the presence and absence of the turbulence generator, are plotted in Fig. 2.13. The general trend of increasing (and subsequent decrease near the trailing edge) plate temperature from the leading edge is clear. To take a closer look, the centerline temperature is plotted in Fig. 2.14a-d; noting that the uncertainties are approximately ±1°C. It can be seen that with increasing distance from the leading edge, the surface temperature rises, this may be partly due to the thickening of the boundary layer and the accumulation of thermal energy. Toward the end of the heated plate, the surface temperature decreases, presumably due to the trailing edge effect.

The qualitative trend appears unchanged with variation in wind speed over the studied range. The overall (absolute) temperature, however, decreases from Fig. 2.14a to Fig. 2.14d. This is primarily due to the increased convection with increasing wind. For all four wind speed cases considered, we see that the turbulence generator (fin) seems to promote the local heat transfer rate, i.e., lowers the surface temperature, except near the trailing edge.

The heat transfer coefficient can be determined from the Newton's cooling law [31],

$$q_x = h_x(T_s - T_\infty) \quad (1)$$

where q_x is local heat flux, T_s is the surface temperature, and T_∞ is the temperature of free stream air. In this study, the local heat flux was quantified using a Hukseflux heat flux sensor. The equation for converting the measured voltage to watt per square meter is

$$q_x = C \times v \quad (2)$$

According to the manufacturer, the constant C is 96, and v is the output voltage. The local Nusselt number is thus

$$Nu_x = \frac{h_x X}{k} \quad (3)$$

where k (Wm^{-1} $°C^{-1}$) is the thermal conductivity of the air at the film temperature ($T_f = \frac{T_s + T_\infty}{2}$) [31].

For a uniform flow over a smooth plate, the transition from laminar to turbulent can be characterized by Reynolds number, which at a distance x from the leading edge of the flat plate is

$$Re_x = \frac{Vx}{\vartheta} \quad (4)$$

where ϑ (m^2/s) is the kinematic viscosity of the air at the film temperature. The value of the critical Reynolds number, where transition into a turbulent boundary layer occurs for a flat plate is around 5×10^5. With a streamwise dimension of 522 mm and $T_{air} \approx 23$ °C, the critical velocity, $V_{cr} \approx 14.4\ m/s$. Thus, the unperturbed flow in this study is expected to remain largely in the non-turbulent regime over the range of tested velocities.

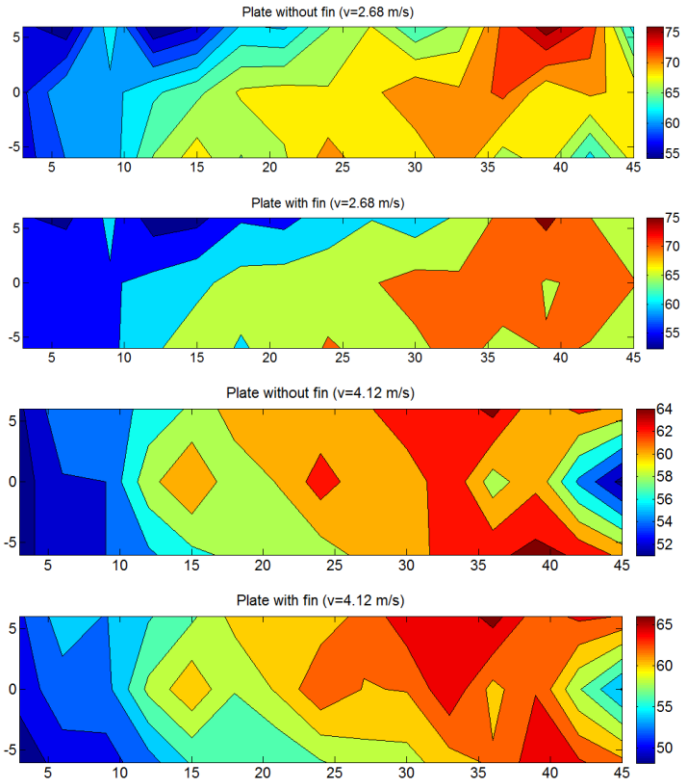

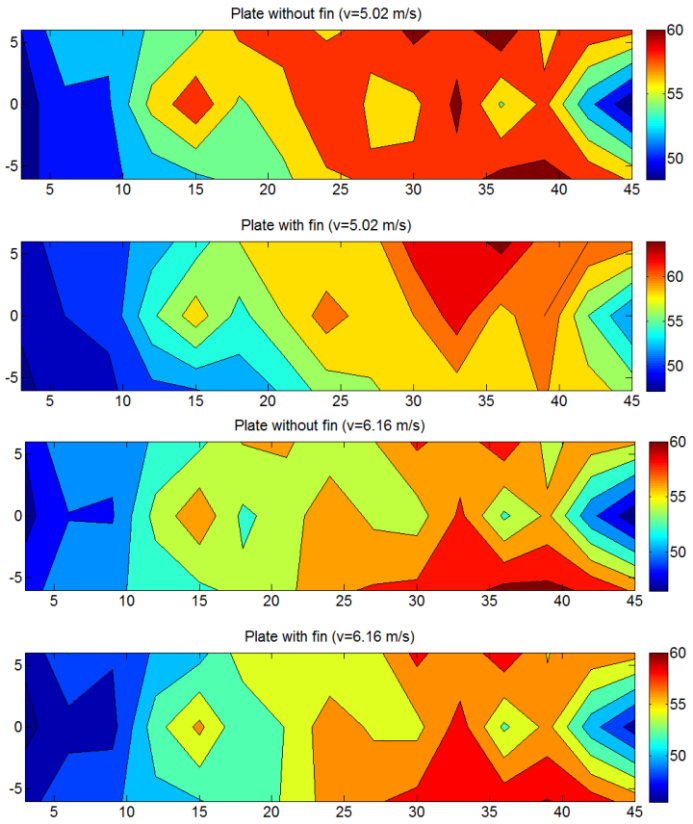

Figure 2.13: Temperature contours for various velocity with and without the turbulence generator (x=0, y=0 is at the middle of the leading edge of the plate, dimensions are in centimeter).

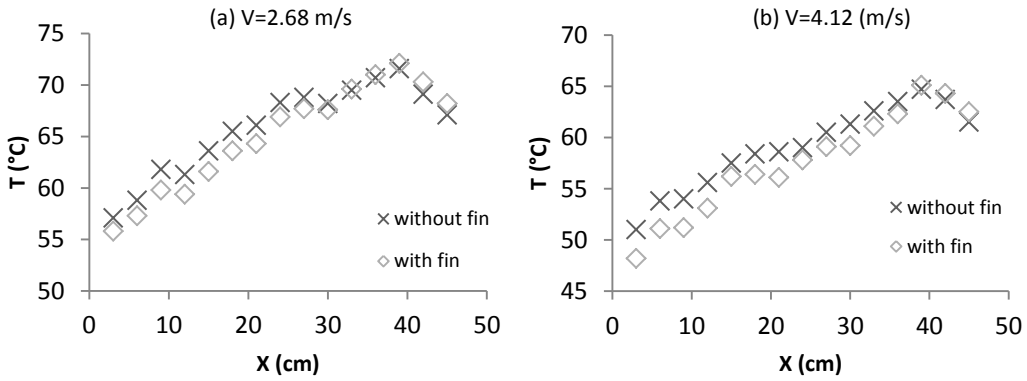

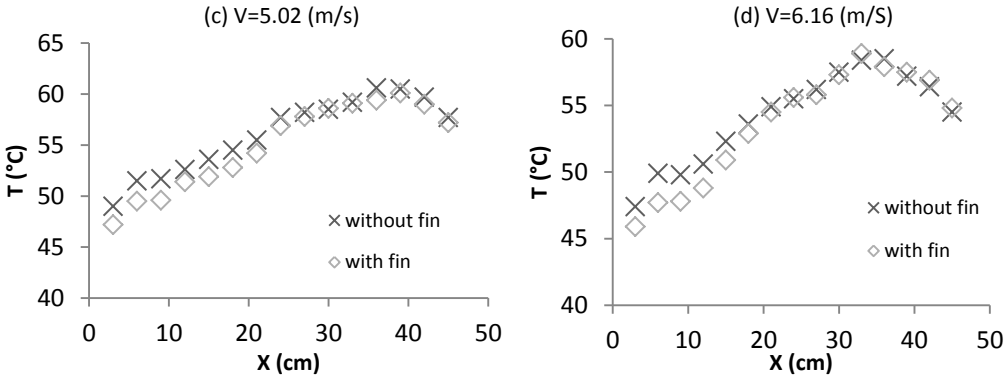

Figure 2.14: Variation of surface temperature along the centerline of the plate without and with the turbulence generator.

The distribution of local heat flux along the centerline of the heated plate in the presence of the turbulence generator (fin) is summarized in Figure 2.15. Other than right after the leading edge and near the trailing edge, the heat flux is somewhat uniform. Comparing this with the temperature distributions in Fig. 2.14a to 2.14d indicates that the condition under investigation is closer to the uniform heat flux condition than the constant surface temperature condition. Fig. 2.15 also depicts a general trend of decreasing heat flux with increasing wind speed.

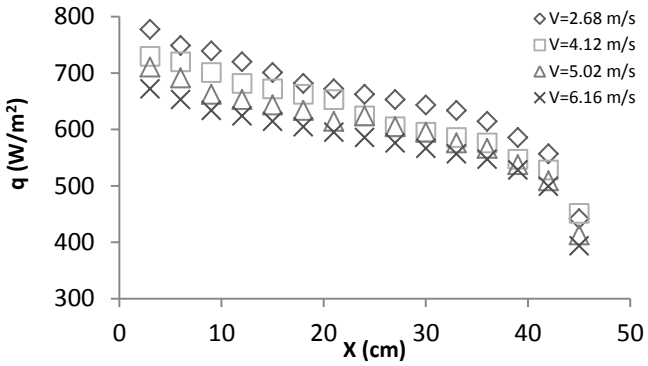

Figure 2.15: Measured heat flux along centerline of plate with turbulence generator (fin).

The corresponding local heat transfer coefficient along the centerline of the heated plate is plotted against the distance from the leading edge in Fig. 2.16. It is clear that the heat transfer coefficient decreases with distance X, which is primarily due to the thickening boundary layer. As expected, the heat transfer coefficient also increases with wind speed.

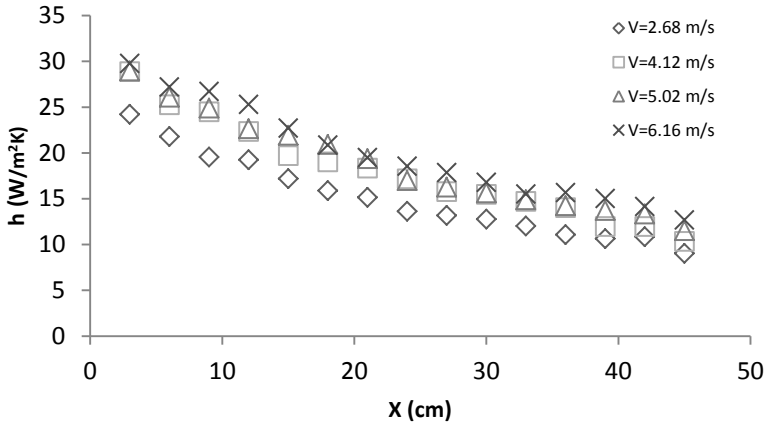

Figure 2.16: Local heat transfer coefficient along the centerline of plate with turbulence generator (fin).

Figure 2.17 portrays the change in the local heat transfer coefficient in the presence and absence of the turbulence generator (fin). Right after the leading edge, which is just downstream of the fin for the finned case, there is a clear enhancement in the heat transfer coefficient in the presence of the turbulence generator. The positive fin enhancement is lost farther downstream. This change from positive heat transfer augmentation to a negative one occurs much sooner and significantly more severely with decreasing wind speed. The main cause for the decay in convection coefficient is likely the decrease in the local wind speed over the heated plate in the presence of the obstructing fin. Thus, the ideal turbulence generator should not impose too much flow restriction. In other words, a good heat transfer enhancer should draw in more fluctuating free stream wind over the surface to be cooled.

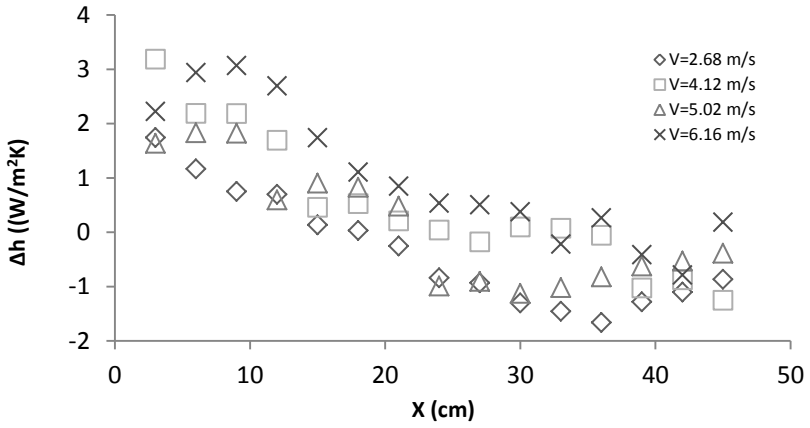

Figure 2.17: Local heat transfer coefficient difference ($\Delta h = h_{fin} - h$).

The average convection coefficient for the length of the heated surface under consideration can be deduced as [31]

$$\bar{h} = \frac{1}{L}\int_0^L h_x dx \quad (5)$$

$$\bar{h} = \frac{1}{n}\sum_{i=1}^{n} h_x \quad (6)$$

The values of this average convection heat transfer coefficient are summarized in Table 2.1; where $\overline{h}_{fin}$ and $\overline{h}$ are the average convection heat transfer coefficients for the flat plate with fin (turbulence generator) and without fin, respectively. A quick comparison reveals that the average convection heat transfer coefficient increases 2, 3.5, 3.4, and 6.2 percent when a fin (turbulence generator) is placed at the leading edge of the plate for free stream velocities of 2.68, 4.12, 5.02, and 6.16 m/s, respectively.

Table 2.1: Average convection heat transfer coefficient

V (m/s)	2.68	4.12	5.02	6.16
$\overline{h}_{fin}$(W/m^{2}K)	15.8	18.5	19.2	20.5
$\overline{h}$ (W/m^{2}K)	15.5	17.9	18.6	19.3

The relation between forced convection coefficient and wind velocity has been studied by many researchers. Among the many wind tunnel studies, MacAdams [32], Watmuff [33], and Sparrow et al [22] are three notable ones relevant to solar panel cooling. Table 2.2 is a summary of the curve fits of these studies. These correlations, along with the well-known Nusselt equation [34] are plotted in Fig.2.18. It is clear that the Nusselt expression gives the smallest heat transfer coefficient for any given wind speed, possibly due to the fact this expression was deduced using laminar wind tunnel data with few disturbances, far from practical conditions. The present study is also conducted in a wind tunnel. However, the current heated plate is not under isothermal nor perfectly uniform heat flux conditions. Moreover, the approaching wind has some background turbulence. This and the flow disturbance caused by the leading edge can lead to higher convection heat transfer coefficients compared to those calculated by the Nusselt equation. The current average heat transfer coefficient results fall within the range of other wind tunnel studies.

Table 2.2: Forced convection relationships (in SI units) deduced from wind tunnel measurements.

MacAdams [32]	Watmuff [33]	Sparrow et al [22]	Nusselt Relation [34]
$h = 3.8V + 5.7$	$h = 3.0V + 2.8$	$h = 4.96V^{0.5}L^{-0.5}$	$\overline{Nu} = 0.664Re^{\frac{1}{2}}Pr^{\frac{1}{3}}$

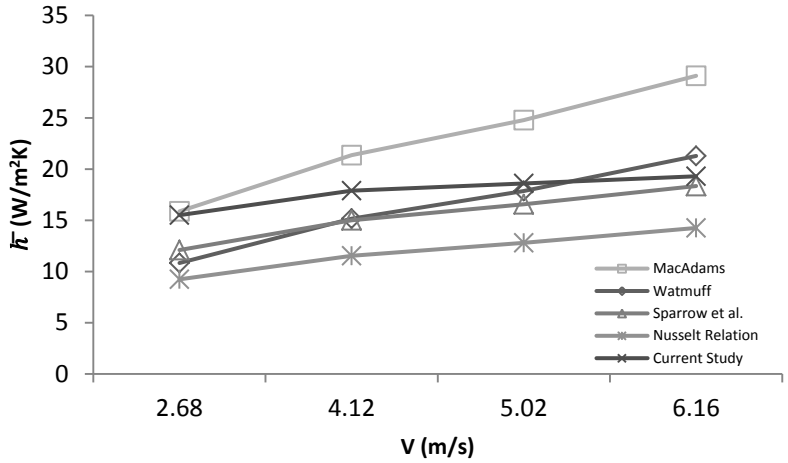

Figure 2.18: Heat transfer coefficient comparison with other wind tunnel measured correlations.

In forced convection heat transfer, it is a common practice to express the heat transfer coefficient in terms of Reynolds number and Prandtl number [35]

$$Nu_x = CRe_x{}^m Pr^n \quad (7)$$

With the Prandtl number approximately fixed at 0.7, we can simplify this into

$$Nu_x = C_1 Re_x{}^m \quad (8)$$

Table 3 summarizes the values of the coefficients C_1 and m of the current finned results as plotted in Fig.2.19. We see that the change with respect to variation in wind speed is small, and hence, we may collapse all the data points unto one curve as shown in Fig.2.20.

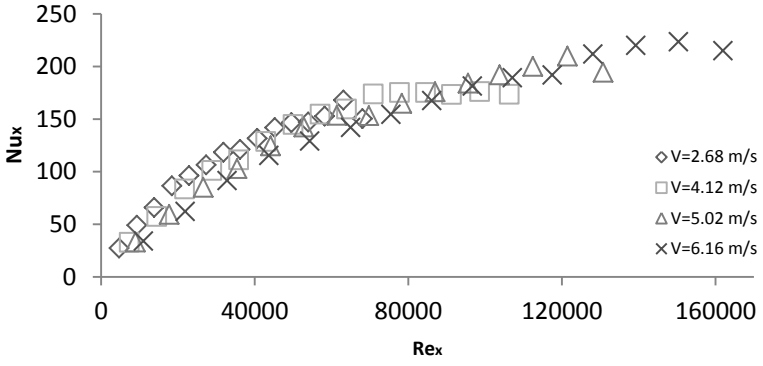

Figure 2.19: Variation of Nussult number with Reynolds number along the centerline of the heated plate with a turbulence generator (fin).

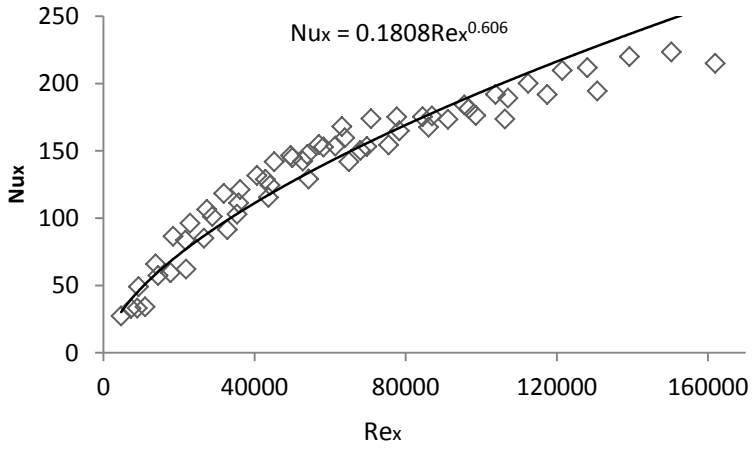

Figure 2.20: Overall local Nusselt number versus local Reynolds number with a turbulence generator (fin).

Table 2.3: Coefficient of Eq. 8 for plate with fin upstream of the leading edge

V (m/s)	C_1	m
2.68	0.1378	0.6442
4.12	0.1317	0.6386
5.02	0.0923	0.6638
6.16	0.0715	0.6799

To better see the effect of the turbulence generator on the effectiveness of the local heat transfer, the local Nusselt number in the presence of the turbulence generator (fin) was divided by that without the turbulence generator (fin) in Fig. 2.21. The figure shows that the turbulence generator (fin) has a positive effect in enhancing Nu just after the leading edge (turbulence generator), but farther downstream along the plate, the turbulence generator actually has a negative effect. The uncertainty associated with the normalized Nusselt number is around 5%. Hence, most of the larger than uncertainty positive to negative turbulence generator effects are real. As postulated earlier, this is probably due to the blockage effect caused by the turbulence generator, i.e., the local wind speed over the heated plate is reduced. Efforts are being made to quantify this and other effects such as recirculation and wake.

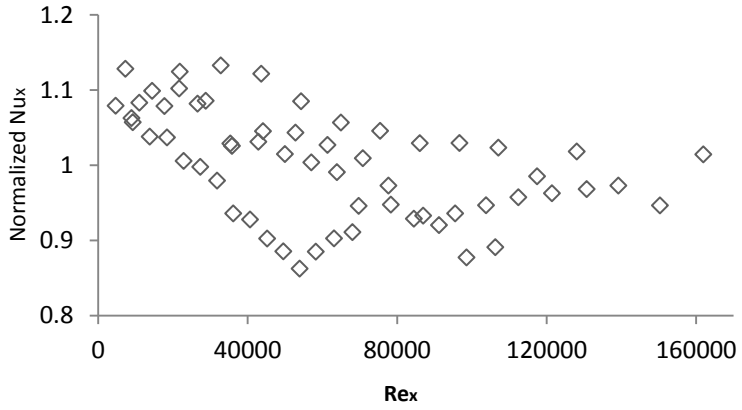

Figure 2.21: Normalized Nusselt number versus Reynolds number.

6. CONCLUDING REMARKS

In this study, an approach to passively cool the PV panel has been initiated. The PV array is modeled by a heated aluminum flat plate placed in a wind tunnel. Temperature distribution and heat flux along the centerline of plate with and without turbulent generator (fin) were measured. The results showed that with the turbulence generator placed at the leading edge, the local surface temperature can be lowered by up to 2°C. While there are locations where the finned local Nusselt number is less than that of the corresponding un-finned one, the averaged Nusselt number over the entire measured streamwise span along the centerline of the plate consistently show a 2 to 6.2 percent increase. Work is underway to better elucidate the underlying fluid mechanics which may be responsible for the variation in local heat transfer effectiveness in the presence of the turbulence generator. As important, efforts are being made to better position and improve the design of the turbulence generator.

ACKNOWLEDGEMENTS

This work was made possible by Natural Sciences and Engineering Research Council of Canada. This is an extension of a project previously sponsored by Ontario Centres of Excellence and Essex Energy Corporation.

REFERENCES

[1] Luque A., Hegedus S. 2nd Ed, Handbook of Photovoltaic Science and Engineering, Wiley, 2011.

[2] National Renewable Energy, Best Research Cell Efficiencies,<http://www.nrel.gov/ncpv/images/efficiency_chart.jpg> , Accessed on April 18, 2013.

[3] Top 10 World's Most Efficient Solar PV Mono-Crystalline Cells, <http://www.solarplaza.com/top10-monocrystalline-cell-efficiency/#Sunpower>, Accessed on April 18, 2013.
[4] Armijo K., Carey V., Gravity-Assisted Heat Pipe With Strong Marangoni Fluid for Waste Heat Management of Single and Dual-Junction Solar Cells, Journal of Solar Energy Engineering, ASME, 135(2): 021016-021016-8, 2013.
[5] Micheli L, Sarmah N, Luo X, Reddy K.S., Mallick K, Opportunities and challenges in micro- and nano-technologies for concentrating photovoltaic cooling: A review, Renewable and Sustainable Energy Reviews, 20: 595-610, 2013.
[6] Kumar R., Rosen M.A., Performance evaluation of a double pass PV/T solar air heater with and without fins, Applied Thermal Engineering 31: 1402-1410, 2011.
[7] Zondag H.A. Flat-plate PV-thermal collectors and systems: a review, Renewable Sustainable Energy Review, 12: 891–895, 2008.
[8] Chow T.T. Photovoltaic/thermal hybrid solar technology: a review, Applied Energy, 87: 365–379, 2010.
[9] Skoplaki E., Palyvos J.A. On the temperature dependence of photovoltaic module electrical performance: a review of efficiency/power correlations, Solar Energy, 83: 614–624, 2009.
[10] Beccali M., Finocchiaro P., Nocke B., Energy and economic assessment of desiccant cooling systems coupled with single glazed air and hybrid PV/thermal solar collectors for applications in hot and humid climate, Solar Energy, 83: 1828–1846, 2009.
[11] Tonui J.K., Tripanagnostopoulos Y. Air-cooled PV/T solar collectors with low cost performance improvements, Solar Energy, 81 (4): 498–511, 2007.
[12] Bambrook S.M., Sproul A.B. Maximising the energy output of a PVT air system, Solar Energy 86 (6): 1857–1871, 2012.
[13] Prasad B.N., Saini J.S. Optimal thermo hydraulic performance of artificially roughened solar air heaters, Solar Energy, 47: 91–6, 1991.
[14] De Vries D.W. Design of a photovoltaic/thermal combi-panel, PhD report, EUT, 1998
[15] Tao H.G., Lee P.S., Hawlader M.N.A., An active cooling system for photovoltaic modules, Applied Energy (90): 309–315, 2012.
[16] SolarWall by Conserval Engineering INC. <http://solarwall.com/en/home.php#>, Accessed on April 18, 2013.
[17] SolarWall by Conserval Engineering INC., <http://solarwall.com/en/products/solarwall-air-heating/solarduct.php>, Accessed on April 18, 2013.
[18] Zhang X., Zhao X., Smitha S., Xub J., Yuc X., Review of R&D progress and practical application of the solar photovoltaic/thermal (PV/T) technologies, Renewable and Sustainable Energy Reviews (16): 599– 617, 2012.
[19] Krauter S. Increased Electrical Yield via Water Flow over the Front of Photovoltaic Panels, Solar Energy Materials & Solar Cells, 82: 31–137, 2004.
[20] Karava P., Jubayer C.M, Savory E., Li S. Effect of incident flow conditions on convective heat transfer from the inclined windward roof of a low-rise building with application to photovoltaic-thermal systems, Journal of Wind Engineering and Industrial Aerodynamics, 104–106: 428–438, 2012.
[21] Bambara, J., Experimental study of a facade-integrated photovoltaic/thermal system with unglazed transpired collector. M.Sc. Thesis, Department of Building, Civil and Environmental Engineering, Concordia University, Montreal, Canada, 2012.

[22] Sparrow E.M., Ramsey J.W., Mass E.A. Effect of finite width on heat transfer and fluid flow about an inclined rectangular plate, Trans. ASME J. Heat Transfer 101: 199–204, 1979.
[23] Wang X.A., An experimental study of mixed, forced, and free convection heat transfer from a horizontal flat plate to air, Trans. ASME J. Heat Transfer 104: 139–144, 1982.
[24] Francey J.L., Papaioannou J. Wind-related heat losses of a flat-plate collector, Solar Energy 35: 15–19, 1985.
[25] Ito N., Kimura K., Oka J. A field experiment study on the convective heat transfer coefficient on exterior surface of a building, ASHRAE Trans. 78: 184–191, 1972.
[26] Sharples S., Full-scale measurements of convective energy losses from exterior building surfaces, Build. Environ. 19: 31–39, 1984.
[27] Loveday D.L., Taki A.H. Convective heat transfer coefficients at a plane surface on a full-scale building facade, Int. J. Heat Mass Transfer 39 (8): 1729–1742, 1996.
[28] Clear R.D., Gartland L., Winkelmann F.C. An empirical correlation for the outside convective air-film coefficient for horizontal roofs, Energy and Building. 35:797–811, 2003.
[29] Hagishima A., Tanimoto J. Field measurements for estimating the convective heat transfer coefficient at building surfaces, Build. Environ. 38 (7): 873–881, 2003.
[30] Palyvos J.A, Survey of wind convection coefficient correlations for building envelope energy systems' modeling: a review, Applied Thermal Engineering 28: 801–808, 2008.
[31] Cengel Y., 2nd Heat Transfer: A Practical Approach, McGraw-Hill Higher Education, 2003.
[32] McAdams W.H., Heat Transmisson, 3rd ed. McGraw-Hill, New York, 1954.
[33] Watmuff J.H., Charters W.W.S, Proctor D., Solar and Wind Induced External Coefficients Solar Collectors 2nd Quarter. Revue Internationale d'Heliotechnique, 1977.
[34] Incropera F.P, DeWitt D.P, Fundamentals of Heat and Mass Transfer. John Wiley & Sons, 2002.
[35] Oosthuizen P.H., Naylor D. Introduction to convective heat transfer analysis. McGraw-Hill, New York, 11–15, 1999.

CHAPTER 3

AN EXPERIMENTAL INVESTIGATION ON PASSIVE COOLING OF A SURROGATE PHOTOVOLTAIC PANEL

I.Arianmehr*

Turbulence & Energy Lab, Centre for Engineering Innovation
University of Windsor, Windsor, Ontario, Canada

D. S-K. Ting

Turbulence & Energy Lab, Centre for Engineering Innovation
University of Windsor, Windsor, Ontario, Canada

S. Ray
Essex Energy Corporation

Oldcastle, Ontario, Canada

1. ABSTRACT

One outstanding challenge of the current commercial PV technologies is the reduction in its conversion efficiency with increasing PV panel temperature, which closely corresponds to the period where sunlight is most readily available. In this study, passive cooling of a surrogate PV panel, a heated aluminum flat plate, using a turbulence generator (fin) was conducted in a wind tunnel. Temperature distribution and heat flux along the centerline of the plate with and without the fin at the leading edge were measured. The results showed that significant wind blockage limited the fin to be effective in lowering the plate temperature for a short distance downstream. Detailed flow measurements revealed that the fin generated flow turbulence is superior in augmenting the Nusselt number. To realize its full potential, however, the drastic blockage caused by the current fin design needs to be mitigated.

NOMENCLATURE

h_x	local heat transfer coefficient $(\mathrm{W/m^2{}^\circ C})$
$h_{with\ fin}$	heat transfer coefficient in finned case $(\mathrm{W/m^2{}^\circ C})$
$h_{without\ fin}$	heat transfer coefficient in un-finned case $(\mathrm{W/m^2{}^\circ C})$

* Corresponding Author: iman.arianmehr@gmail.com.

k	thermal conductivity $(\mathrm{W/m°C})$
L	total length of plate in streamwise direction (mm)
N	number of sample points in hotwire measurements
Nu_x	local Nusselt number, based on h_x and streamwise distance from leading edge of plate, $Nu_x = h_x X/K$
Nu_L	local Nusselt number based on h_x and total streamwise length of plate, $Nu_x = h_x L/K$
Pr	Prandtl number
q	heat flux rate (W/m^2)
q_x	local convection heat transfer(W/m^2)
Re_x	Reynolds number based on streamwise distance, $Re_x = U_\infty X/\vartheta$
Re_L	local Reynolds number based on the average local velocity, $Re_L = U^* L/\vartheta$
T_f	film temperature (°C)
T_s	measured surface temperature (°C)
T_∞	free stream temperature (°C)
Tu	turbulence intensity, $Tu = \frac{u_{rms}}{U_\infty}$
Tu_L	local turbulence intensity, $Tu_{mean} = \frac{Tu_{(Y=5\ mm)} + Tu_{(Y=10.5\ mm)}}{2}$
u_i	instantaneous velocity (m/s)
u_{rms}	root-mean-square of the velocity fluctuation (m/s)
U_∞	free stream velocity (m/s)
U^*	average local velocity, $U^* = \frac{u_{(y=5\ mm)} + u_{(y=10.5\ mm)}}{2}$
$\overline{U}$	time averaged velocity (m/s)
X	streamwise distance from the leading edge (cm)
y	vertical position from the surface (mm)
Δh	local heat transfer coefficient difference ($\Delta h =$

	$h_{with\ fin} - h_{without\ fin}$), (W/m^2°C)
ΔU^*	difference between dimensionless velocity profiles, $\Delta U^* = (\frac{u}{U_\infty})_{without\ fin} - (\frac{u}{U_\infty})_{with\ fin}$
ΔTu	difference of local turbulence intensity, $\Delta Tu = (Tu)_{without\ fin} - (Tu)_{with\ fin}$

Greek Symbols

δ	boundary layer thickness (mm)
ρ	density (kg/m^3)
μ	dynamic viscosity (kg/m·s)
ϑ	kinematic viscosity (m^2/s)

2. INTRODUCTION

Solar energy is one of the most promising sources of energy, since it can supply clean, environmentally friendly and inexhaustible energy [1]. Conversion of solar radiation directly into electricity through PV (photovoltaic) cells is one of the fastest-growing applications of capturing the sun's energy. An estimation for the energy payback period for modern PV cells is 1-4 years [2]. Further, with the lifespan of a typical PV cell between 20 and 30 years, they can also be effective and profitable energy generators.

The maximum theoretical efficiency of a solar cell is determined by the Shockley–Queisser limit. The maximum efficiency of a single layer p-n junction solar cell with the band gap of 1.37 eV is 33.7% [3]. Since the band gap of silicon, which is the most popular semiconductor for producing PV cell, is about 1.1 eV, the maximum achievable conversion efficiency of a single layer p-n junction of this kind of PV cell is about 29% [1]. Fierce efforts have been made, in order to enhance the efficiency of PV cells and decrease the manufacturing costs.

At present, the best non-concentrator mono crystalline silicon cells with small dimensions (2 cm × 2 cm) have a laboratory operating efficiency of approximately 25%. The world's highest module efficiency is about 23%, while concentrator multi-junction cells have a demonstrated efficiency as high as 44% in a well-controlled laboratory environment [4]. Typical mass-produced commercial mono-crystalline PV cells have an efficiency of less than 22.5% in field applications [5]. Thus, only a fraction of the absorbed sunlight is converted into electricity. The majority of incident solar is converted to heat, which increases the cell's temperature. This can lead to decreasing efficiency of the PV

cells [6,7]. Also, in the long term, permanent damage and structural failure of solar PV panels (or "modules") such as degradation due to prolonged thermal stress is considered irreversible [8,9]. Therefore, it is beneficial to remove waste heat, thus improving the performance of PV modules while prolonging their life time.

Cooling of PV modules can be achieved by utilizing a fluid stream such as water or air. The extracted heat from the coolant fluid can be utilized for other useful applications. This has led to the development of PV-Thermal (PVT) systems which are generally hybrid solar PV and solar thermal collectors. The PVT research work falls into four major classifications: (1) air-type PVT [10,11], (2) water-type PVT [12-14], (3) refrigerant-type PVT [15,16], and (4) heat pipe-type PVT [17]. The last two methods, (3) and (4), are in relatively early stages of research and still require more development in order to become commercially – or even technically – viable. However, significant advancement has been accomplished in both air-type and water-type PVT systems [18]. In this case, the water PVT collectors are similar to conventional flat plate collectors whose absorbers are covered by an appropriate PV layer [19]. The aim of this system is to maximize the performance of PV cells by distributing the thermal energy into the flowing coolant while converting solar radiation to electricity [20].

Krauter [21] studied the effect of a flowing film of water on the surface of PV cell by placing a series of nozzles at the top of the module. In addition to cleaning the surface of the module, the film of water decreased the reflection of sunlight by 2-3.6%. Also observed was a reduction in cell temperature of up to 22°C.

The feasibility of impinging jet cooling of densely packed PV array was investigated by Royne and Dey [22]. The impinging jets assist in leveling out the non-uniformity in heat transfer coefficient which reduces the performance of PV cells. Also, it was concluded that the impinging liquid jet is more effective for scattering the generated heat from densely packed photovoltaic cells.

Tonui and Tripanagnostopoulos [23] used a suspended metal sheet at the middle of an air channel to improve the performance of air-cooled PVT. The relation between heat output and temperature rise of various PVT designs was investigated by Bambrook and Sproul [24]. In order to improve heat transfer from PV modules, Kim et al. [25] proposed module surface cooling using water circulation and the results showed an improvement of 11.6% in maximum output power. Rahou et al. [26] studied the performance of integrated photovoltaic thermal roofing with an oscillatory flow. Kumar and Rosen [7] evaluated the performance of a double pass PV/T solar air heater with and without fin. The temperature of the PV module was reduced by installing an extended surface on the back of the absorber and subsequently the performance of the module increased. Tao et al. [27] experimentally and numerically showed that by employing a fin in a duct flow and fabricating the duct at the back of the PV module, the electrical efficiency of a PV cell can increase from 8.6% to 12.5%.

A novel cooling method for PV cells under concentrated radiation was adduced by Liu et al [28]. They proposed increasing heat transfer from both the front and back of

the solar panel by directly immersing the cells in dimethyl-silicon oil, a dielectric liquid. The light source was provided by a long-arc xenon lamp. The results showed a uniform temperature distribution with a maximum temperature difference of only 3°C.

In the aforementioned methods, which can be categorized as active cooling, some amount of electric power is required to stream the coolant. In other words, some part of the acquired power is needed to run a pump or blower for circulation of the cooling fluid, and accordingly, lowers the overall electrical efficiency of the PVT system. Thus, minimizing the required pumping power is a significant consideration when designing a PVT system. Also, in order to maintain a minimum level of performance of PV cells, the outlet temperature of the coolant should be sufficiently low (<40°C) [29]. For this reason, the heat produced from PVT systems can be used only in low temperature heat demand applications, such as domestic hot water production, floor heating, and desiccant cooling [30].

Wind-induced convection heat transfer has been evaluated by many researchers. The effect of incident flow conditions on forced convective heat transfer from an integrated PVT system on an inclined roof has been studied by Karava et al. [31]. Bambadra [32] investigated the efficiency of corrugated an unglazed transpired solar collector combined with a photovoltaic system. An increase of 70% in the efficiency of the system was revealed. Selecting the most appropriate available wind-convection heat transfer correlations in the literature for a particular application depends on parameters including the characteristic lengths, wind speed, wind turbulence, wind direction, etc. Some of the available data are based on wind tunnel studies for relatively small plates [33-35], while others were acquired in full scale field tests with actual buildings [36-40]. Furthermore, there have been attempts, such as that made by Palyvos [41], to try to put the wide range of results into perspective. Qualitatively, the general consensus is that heat transfer is enhanced by increasing wind speed and/or turbulence intensity. There are, however, significant discrepancies regarding the quantitative effects.

Developing a passive cooling method for PV panels by enhancing the wind induced convective heat transfer can increase the conversion efficiency of PV cells. External power is not required in this method. Convincing simplicity as well as a reduction in initial, operational, and maintenance costs are promised. In addition, the design of devices that promote passive cooling methods may be easy to retrofit onto the fixtures of existing PV modules. Thus, the objective of this study is to characterize the local Nusselt number with the corresponding local Reynolds number and flow turbulence for fluid flow over a heated flat plate.

3. EXPERIMENTAL SETUP

The solar panel was surrogated by a 522 mm by 337 mm aluminum flat plate. To control the surface temperature of the flat plate, a 457.2 mm × 304.8 mm silicone-rubber heating pad was fitted underneath the plate and connected to a DC power supplier. At steady state condition, the input energy to the plate is equal to the energy which is transferred from the flat plate to the free stream via convection (Q_{conv}), conduction (Q_{cond}) and radiation (Q_{rad}) (Fig. 3.1). A carbon fiber cloth and a particle board were

employed to insulate the bottom from the surrounding and hence, reduce the heat loss from the back of the plate. The dimensions of the flat plate and the rubber heater underneath of plate are illustrated in Fig. 3.2.

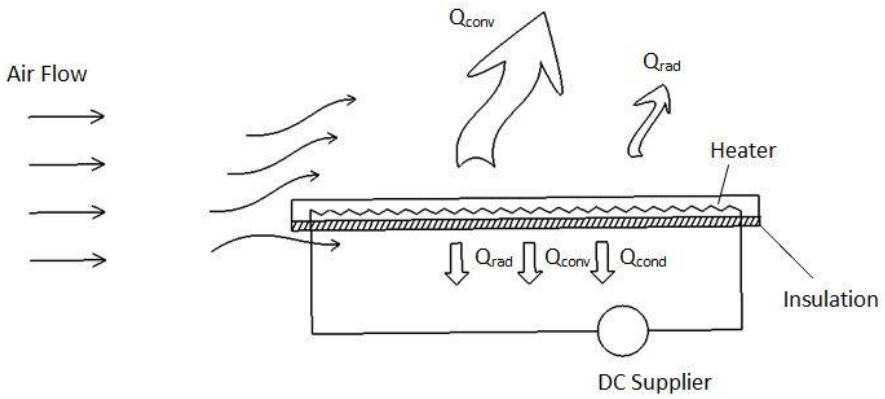

Figure 3.1: Energy balance under steady state condition.

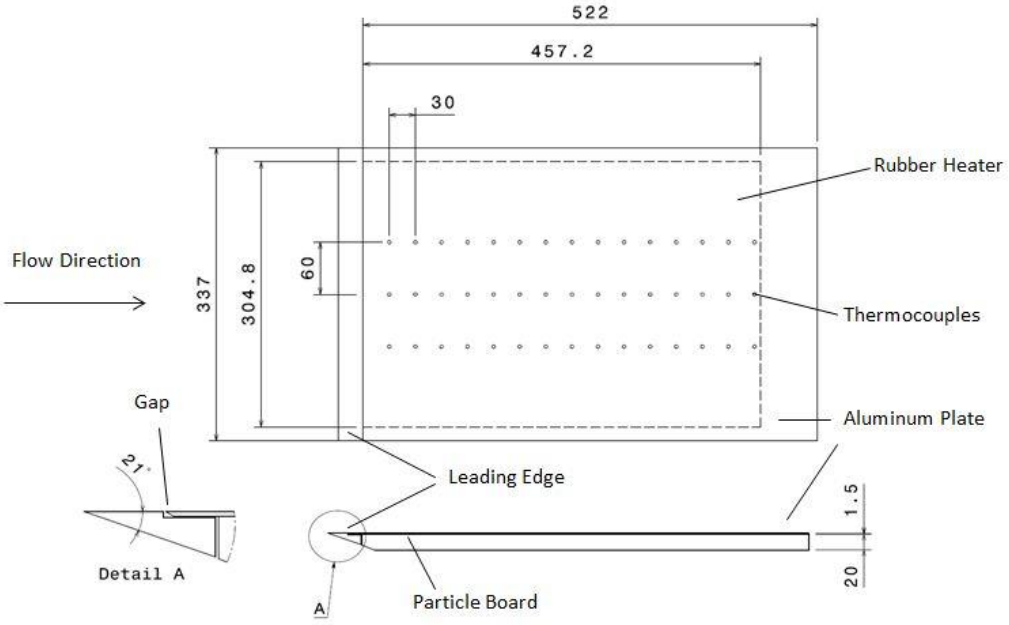

Figure 3.2: Configuration of the flat plate (dimensions are in mm).

The surface temperature distribution was monitored by 45 type T thermocouples mounted on the back of the aluminum sheet as shown in Fig. 3.2. Thermocouple adhesive pads were used to secure wire probes to the surface. The distances between two consecutive rows or columns are 3 cm and 6 cm, respectively. This particular distribution aims at maximizing the coverage over the area of interest, away from the two sides. The local heat flux was measured by a heat transfer sensor manufactured by Hukseflux, model PU-11 which has an accuracy of ±5%.

The complete experimental setup is shown in Fig. 3.3a. A turbulence generator made of Plexiglas with a thickness of 6 mm as detailed in Fig. 3.3b was employed, aiming

to significantly enhance the incoming wind turbulence. The solidity ratio of the turbulence generator was 43%. It was attached to the leading edge of the heated plate as portrayed in Fig. 3.3a. The plate was placed at the half height and in the middle of the test section. The free stream velocity in the wind tunnel was monitored by a Pitot-static tube, which was connected to a digital manometer (Dwyer series 475 mark II).

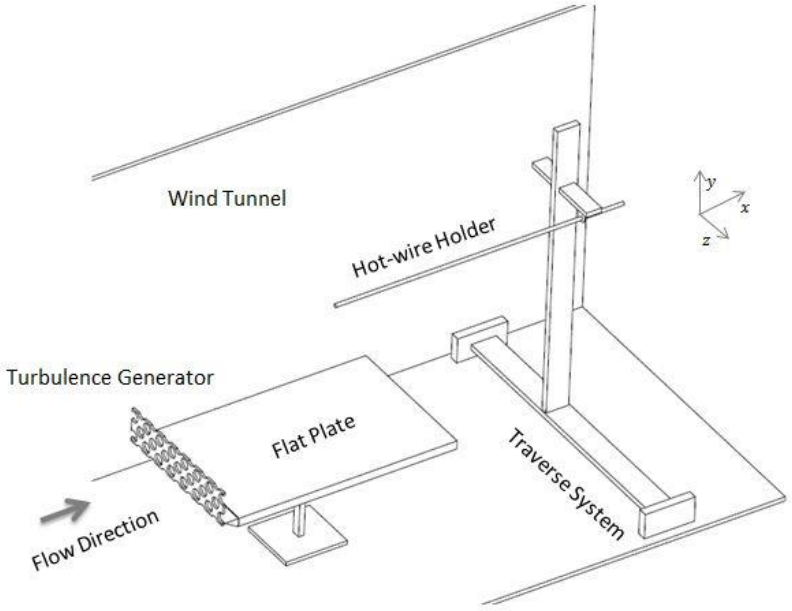

(a)

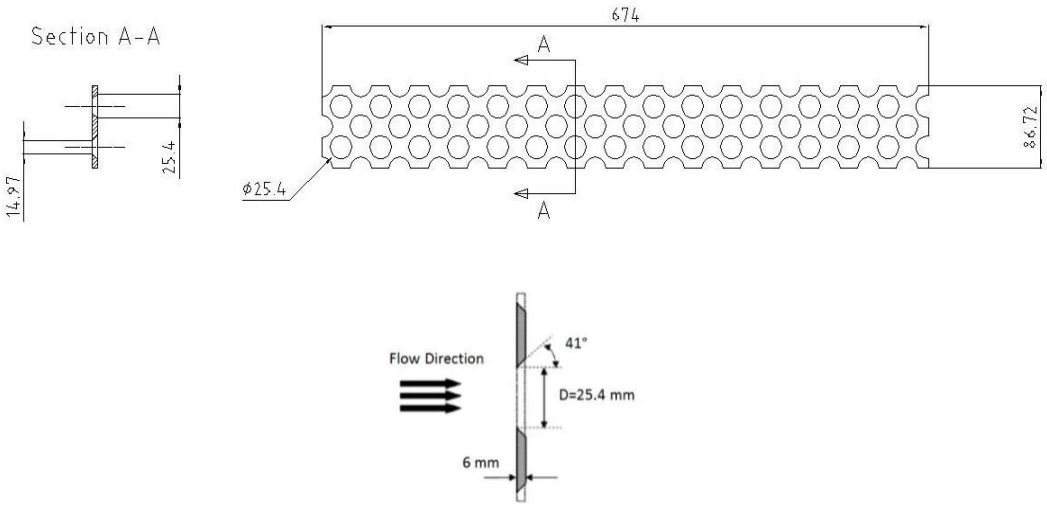

(b)

Figure 3.3: Experimental setup (a) layout in the wind tunnel (b) geometry of the turbulence generator (dimensions are in mm).

4. DATA COLLECTION

The experiments were conducted in a closed-loop horizontal wind tunnel. The test section of the wind tunnel roughly measures 1.8 m long with a cross section of 0.76 m × 0.76 m. A preliminary test was accomplished at the wind tunnel to determine the velocity profile and background turbulence level. Velocity measurements were performed while traversing a hot-wire probe over 15×50 points (horizontally and vertically as depicted in Fig. 3.4) at the leading edge of the surrogate solar panel (a heated flat plate) in the absence of the panel. The air velocity and turbulence intensity were quantified using a Dantec constant temperature anemometer (CTA) module 90C10 with a Dantec Type 55P11 one dimensional straight probe. It has a 5 µm diameter, 1.25 mm active length platinum-plated tungsten wire sensor. The analog voltage signals were first low-passed at 30 kHz using an analog filter to avoid aliasing and were sampled at 80 kHz over 25 s periods (Sample Number = 2,000,000) through a 12 bit PCI-6071E National Instrument data acquisition card.

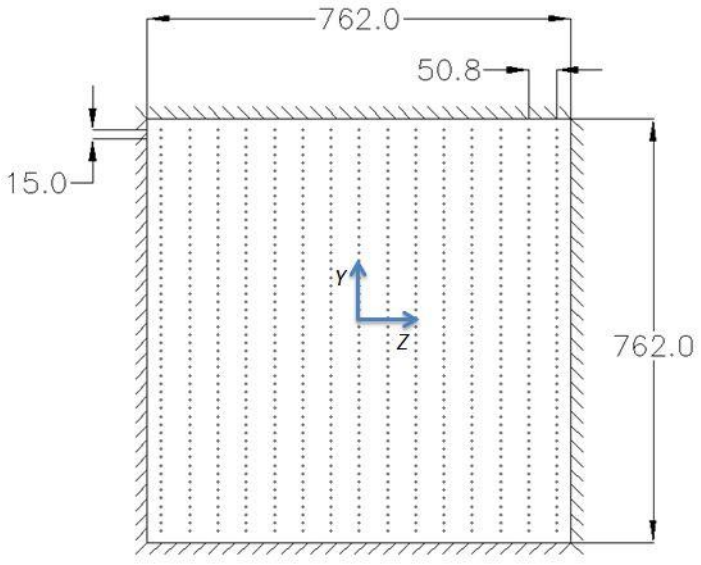

Figure 3.4: Cross section of the test section, looking downstream, positive X (pointing in). The dots signify the measurement points (dimensions are in millimeters).

The velocity was measured as a series of discrete points, u_i. The mean velocity, $\bar{U}$, is defined as the time average of instantaneous measured velocities at each location. Turbulent fluctuation is defined as the difference between instantaneous velocity and time averaged velocity. The root-mean-square velocity is calculated as:

$$u_{rms} = \sqrt{\sum_{i=1}^{N} \frac{(u_i - \bar{U})^2}{N-1}} \qquad (1)$$

where sample size N=2X10^6. The relative turbulence intensity is

$$Tu = \frac{u_{rms}}{U_\infty} \times 100\% \qquad (2)$$

where U_∞ is the free stream velocity.

The velocity in the X (flow stream) direction is plotted as a function of the Y-Z coordinate as shown in Fig. 3.5. It is clear that the velocity profile for the entire cross section outside the boundary layer is reasonably flat. It can be observed that the largest turbulence intensity in this cross section is less than 0.5%, with an average value of approximately 0.4%

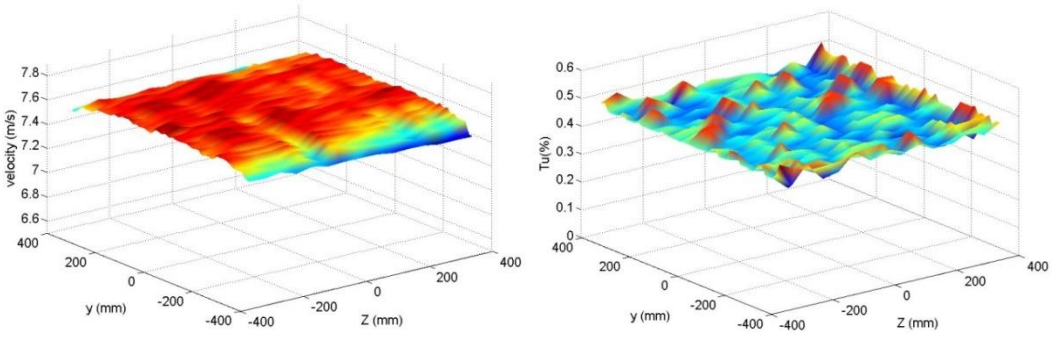

Figure 3.5: Air velocity and turbulence intensity profile in the empty test section (15×50 grid point measurement).

The heat transfer coefficient can be determined from the Newton's cooling law [42],

$$q_x = h_x(T_s - T_\infty) \qquad (3)$$

where q_x is the local heat flux, T_s is the surface temperature, and T_∞ is the temperature of free stream air. In this study, the local heat flux was quantified using a Hukseflux heat flux sensor. The overall diameter of the sensor is 25 mm with sensitive area of 15 mm^2.

5. RESULTS AND DISCUSSION

5.1 HEAT TRANSFER ANALYSIS

The effect of the fin (turbulence generator) on temperature distribution and heat transfer of the plate were examined by placing the fin at the leading edge of plate. Then the results were compared to those obtained without the turbulence generator. After turning the heater and the wind tunnel on, it took approximately two hours for the system to reach equilibrium. The temperature and heat flux were measured five times in 15 minute intervals, and the local temperature and heat flux along the plate were determined by the mean value at each point. The experiments were performed for freestream velocities of 7.3, 10.8, 13.5, 16.1, and 20.9 m/s. Due to space limitation, only results corresponding to 7.3, 13.5, and 20.9 m/s wind are presented and discussed. The center region of the plate is least affected by any side edge effects, and hence, it was chosen for observation. Sample temperature contours along the centre area of the heated plate, 12 cm in width and 45 cm in length, are illustrated in Fig. 3.6. The general tendency of rising temperature over roughly 80% of the plate is followed by declination in temperature near the trailing edge. This trend is observed both in the presence and absence of the turbulence generator at the leading edge of the plate.

In order to have a closer look, the mean temperature at the centerline of the plate with uncertainty of ±1°C is outlined in Fig. 3.7. It can be seen that with increasing distance from the leading edge, the surface temperature rises, this may be partly due to the thickening of the boundary layer and the accumulation of thermal energy. Toward the end of the heated plate, the surface temperature decreases, presumably due to the trailing edge effect and the fact that the heater does not cover the last part of the plate (recall Fig. 3.2). The qualitative trend appears unchanged with variation in wind speed over the studied range. The overall (absolute) temperature, however, decreases with increasing wind speed as depicted in Figs. 3.6 and 3.7. This is primarily due to the increased convection with increasing wind, for a fixed the heat input. For all five wind speed cases considered, we see that the turbulence generator (fin) seems to promote the local heat transfer rate, i.e., lowers the surface temperature up to a distance of approximately 20 cm from the leading edge of the plate. Beyond this point, the effect of the fin on enhancing the cooling of the plate gradually decreases. It can be seen that downstream of this critical distance the temperature of the plate with the fin appears slightly higher than the one without fin, signifying a less effective cooling with the fin farther downstream, or more correctly, the un-finned case is more effective in convective cooling beyond the critical point.

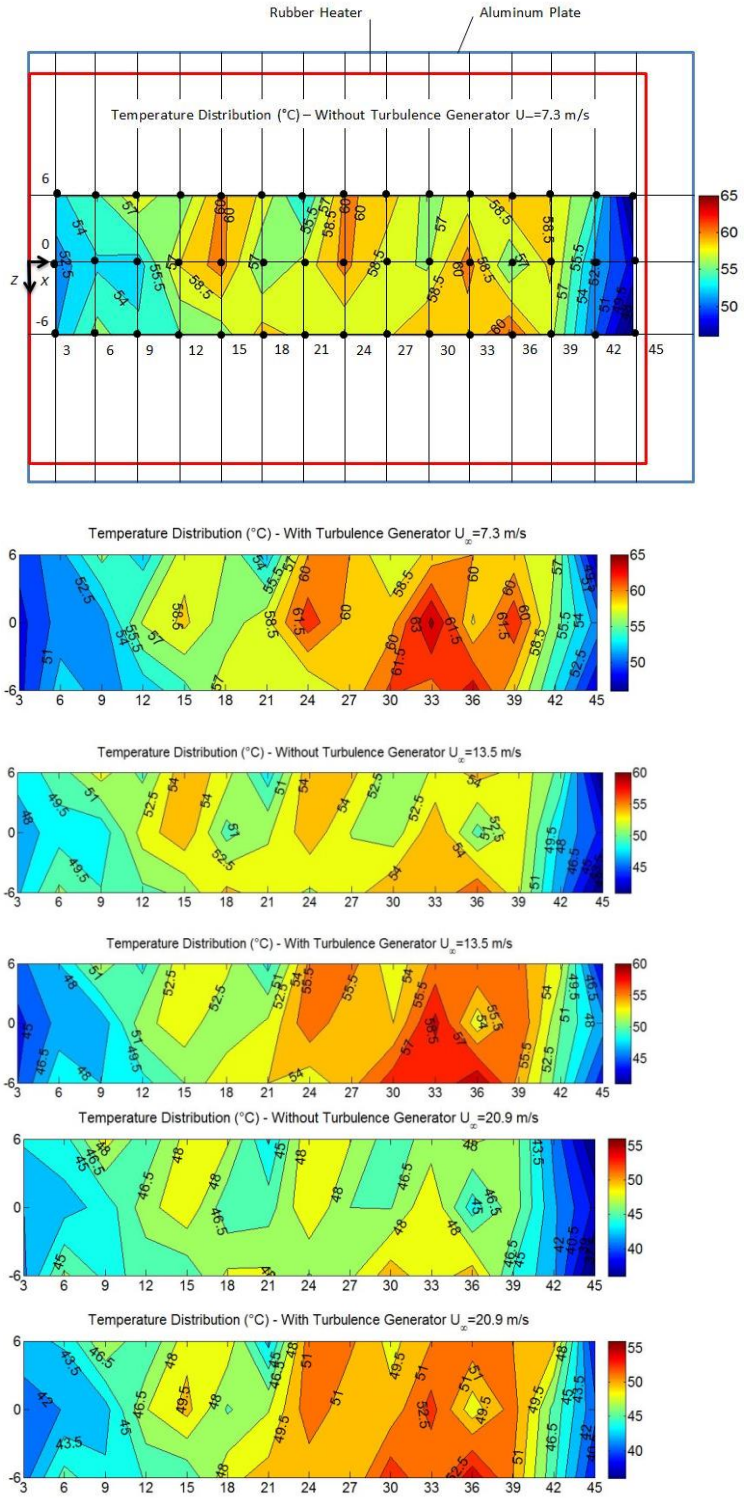

Figure 3.6: Temperature contour in the presence and absence of the turbulence generator (X=0, Y=0 is at the middle of the leading edge of the plate, dimensions are in centimeters).

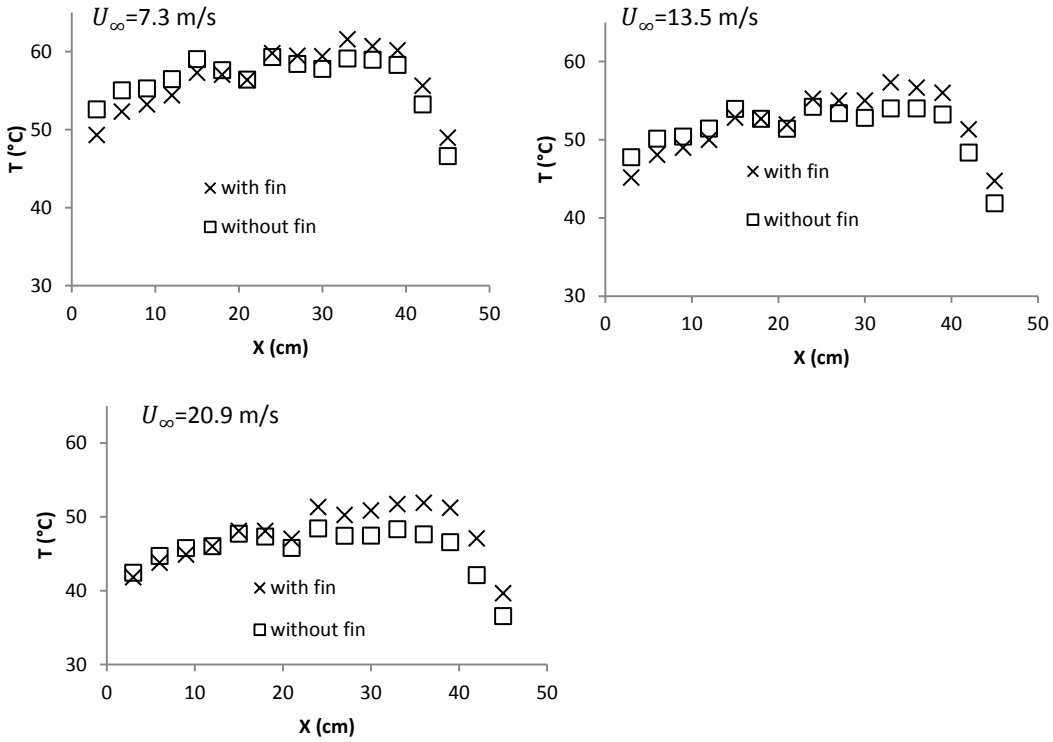

Figure 3.7: Variation of surface temperature along the centerline of the plate without and with the turbulence generator.

The distribution of local heat flux in the presence of the turbulence generator (fin) and in the absence of the fin is summarized in Fig. 3.8. The convection heat flux increases with distance from the leading edge and then decreases as we approach the trailing edge. Figure 3.8 also seems to depict a general trend of decreasing heat flux with increasing wind speed. This is largely due to the decreasing surface temperature with increasing wind speed (Fig. 3.7), for the energy input into the heat pad has been kept the same for all studied cases.

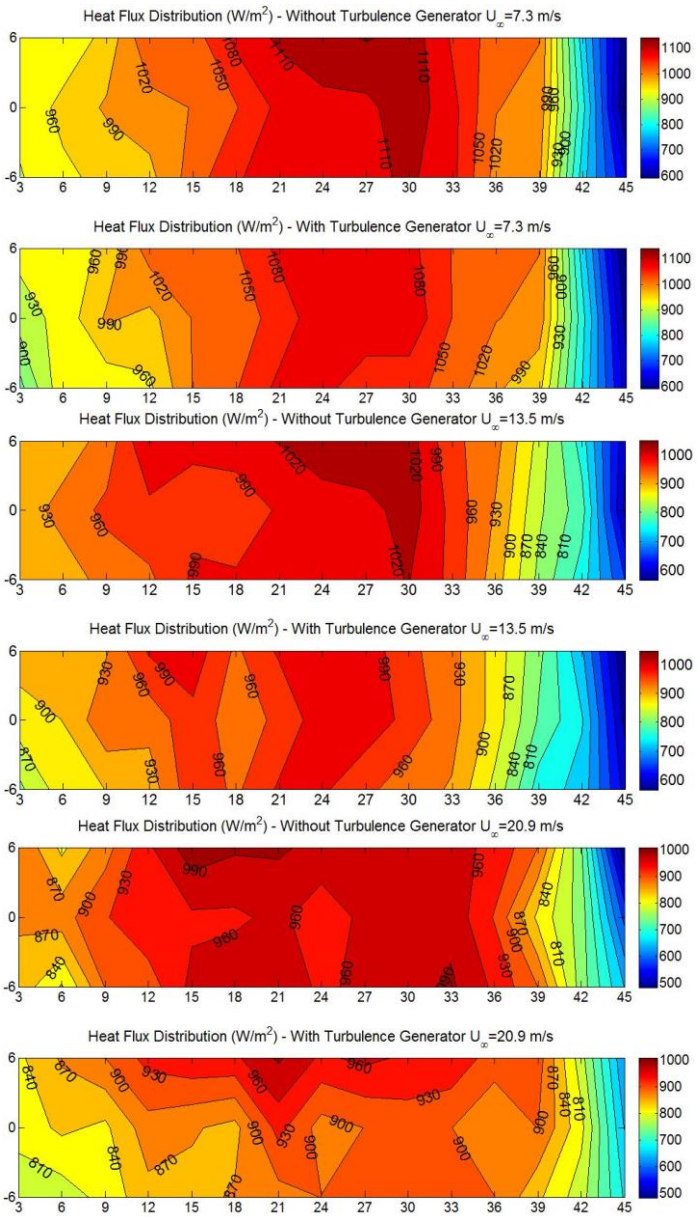

Figure 3.8: Heat Flux contour in the presence and absence of the turbulence generator (X=0, Y=0 is at the middle of the leading edge of the plate, dimensions are in centimeters).

It is clear that the condition is neither uniform surface temperature nor constant heat flux, making clear deduction of what is occuring with respect to the local heat convection from the surface temperature and heat flux distribution results challenging. The more reliable parameter is the local heat transfer coefficient, which has been plotted against distance from the leading edge in Fig. 3.9. It is clear that the heat transfer coefficient decreases with distance X, which is primarily due to the thickening boundary layer. As expected, the heat transfer coefficient also increases with wind speed (note the change in the contour scale with increasing wind speed in Fig. 3.9).

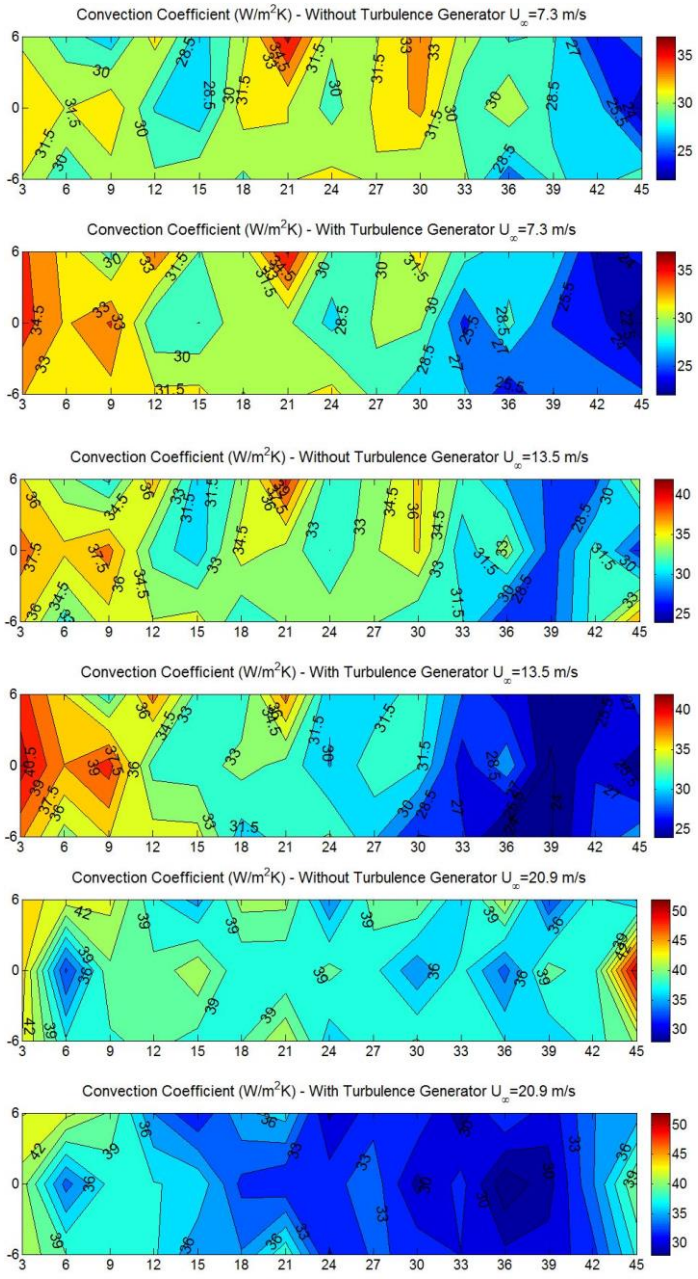

Figure 3.9: Convection coefficient contour in the presence and absence of the turbulence generator (X=0, Y=0 is at the middle of the leading edge of the plate, dimensions are in centimeters).

The mean value of the convection coefficient is defined as the average of the three measured values for the middle strip of the plate at the same streamwise, x location, away from the edge interference. Figure 3.10 presents the variation of this local mean convection coefficient with respect to streamwise distance from the leading edge of the plate in the presence of the turbulence generator (fin) minus that without the fin. Right after the leading edge, which is just downstream of the fin for the finned case, there is a clear enhancement in the heat transfer coefficient in the presence of the

turbulence generator. However, the positive fin-related heat transfer coefficient enhancement is lost farther downstream. This change from positive heat transfer augmentation to a negative one appears to occur sooner and more significantly at the higher wind speeds. This will be examined more closely from the non-dimensional perspective.

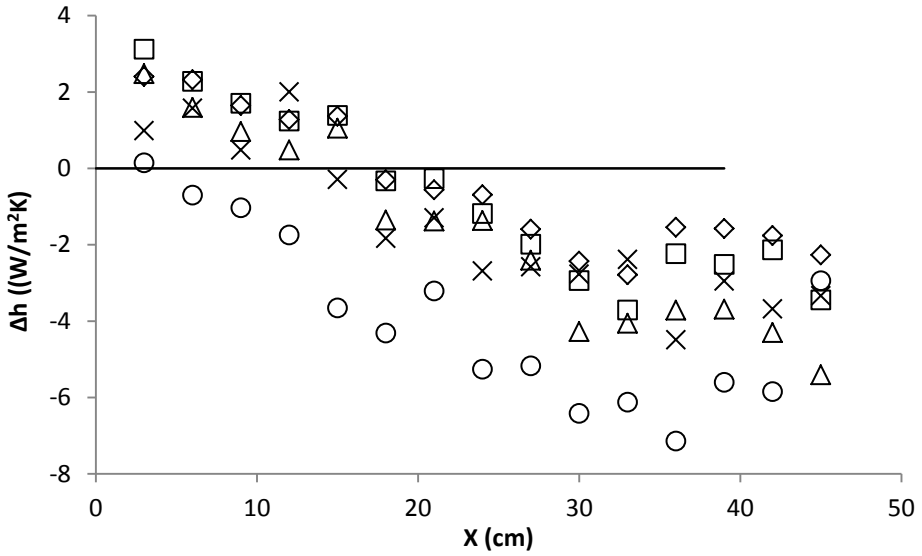

Figure 3.10: Local heat transfer coefficient difference ($\Delta h = h_{with\ fin} - h_{without\ fin}$). (◇, U_∞= 7.3 m/s; □, U_∞= 10.8 m/s; Δ, U_∞= 13.5 m/s; ×, U_∞= 16.1 m/s; ○, U_∞= 20.9 m/s).

The heat transfer coefficient can be determined from $q_x = h_x(T_s - T_\infty)$. The local Nusselt number is thus

$$Nu_x = \frac{h_x X}{k} \qquad (4)$$

where k (W/m°C) is the thermal conductivity of the air at the film temperature ($T_f = \frac{T_s+T_\infty}{2}$) [42]. In forced convection heat transfer, it is a common practice to express the heat transfer coefficient in terms of Reynolds number and Prandtl number [42]

$$Nu_x = C{Re_x}^m Pr^n \qquad (5)$$

With the Prandtl number approximately fixed at 0.7, this can be simplified into:

$$Nu_x = C_1 {Re_x}^m \qquad (6)$$

where Reynolds number is based on the free stream velocity, i.e., $Re_x = U_\infty X/\vartheta$. The relation between local Nusselt number and Reynolds number is depicted in Fig. 3.11. The expected increasing Nusselt number with Reynolds number is clear for both finned and un-finned cases. Also for both finned and un-finned cases, there is a slight lowering of the slope with increasing wind speed. This is consistent with the results shown in Fig. 3.10, possibly due to changing leading edge effect caused by the relatively thick plate (with wedge) which has not been normalized as the wind speed was altered. The lowering of the slope with wind speed is somewhat more prominent for the finned case, this may be because the fin height has also not been adjusted to ensure the appropriate normalized height with respect to the wind speed.

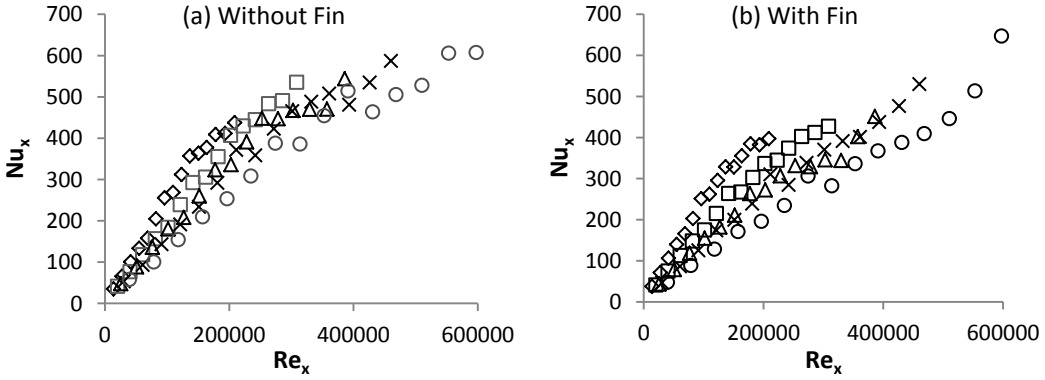

Figure 3.11: Variation of Nusselt number with Reynolds number along the centerline of the heated plate (a) without the turbulence generator (b) with the turbulence generator. (◇, U_∞= 7.3 m/s; □, U_∞= 10.8 m/s; ∆, U_∞= 13.5 m/s; ×, U_∞= 16.1 m/s; ○, U_∞= 20.9 m/s).

To better elucidate the effect of the turbulence generator on the effectiveness of the local heat transfer, the local Nusselt number was normalized in the presence of the turbulence generator (fin) with respect to that without the turbulence generator (fin) in Fig. 3.12.

$$Normalized\ Nu_x = \frac{finned\ Nusselt\ umber}{unfinned\ Nusselt\ number} \qquad (7)$$

The figure shows that the turbulence generator (fin) has a positive effect in enhancing the local Nusselt number just after the leading edge (turbulence generator), but farther

downstream, the turbulence generator actually has a negative effect. The uncertainty associated with the normalized Nusselt number is approximately 5%. The corresponding variation is clearly larger than the uncertainty, and hence, the change from a positive effect to a negative one in the presence of the turbulence generator is real.

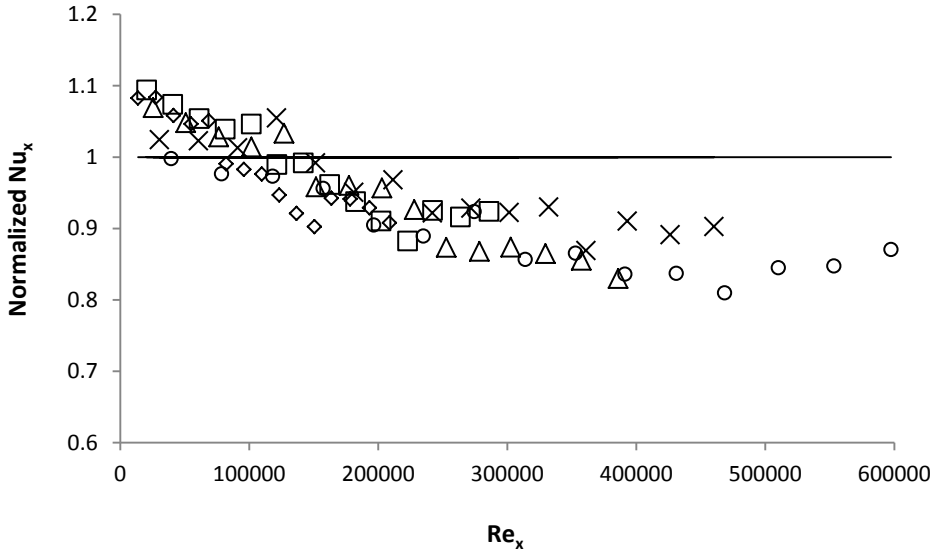

Figure 3.12: Normalized Nusselt number versus Reynolds number. (◇, U_∞= 7.3 m/s; □, U_∞= 10.8 m/s; Δ, U_∞= 13.5 m/s; ×, U_∞= 16.1 m/s; ○, U_∞= 20.9 m/s).

5.2 FLOW CHARACTERISTIC ANALYSIS

We have so far assumed freestream velocity (U_∞) in deducing local Reynolds number. Detailed local flow characteristics are needed to better elucidate the underlying physics behind the Nu_x-Re_x results. By revealing the influence of the turbulence generator and the wedge fixture on the resulting flow, the corresponding heat transfer characteristics can be cast into proper perspective.

Seven streamwise sections and two Z planes (Z=0 and Z=23 mm) as shown in Fig. 3.13 were selected for flow measurements. The first cross-section was 6 cm from the leading edge and the subsequent sections was also 6 cm apart. At each cross-section, measurements were performed at thirty-one points spaced 5.5 mm apart. Due to space limitation, only results at the first, third, fifth, and seventh streamwise cross-sections are presented; the results at the second, fourth and sixth cross-sections fall between the corresponding neighbors.

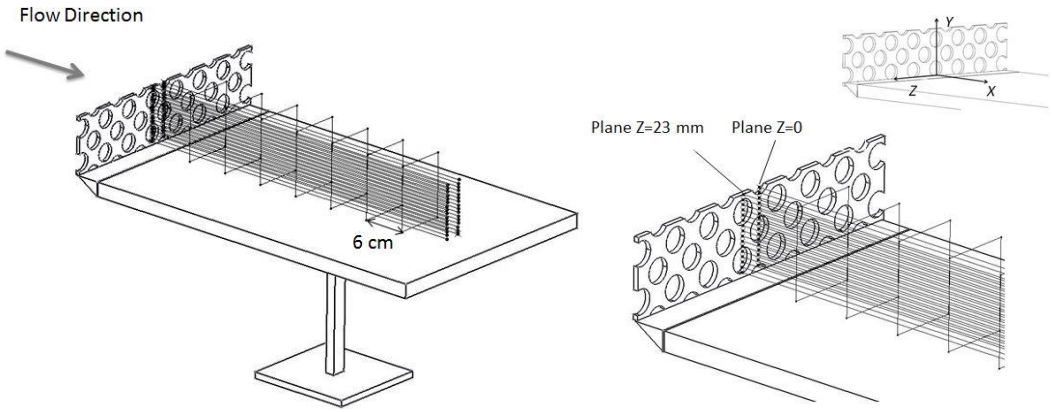

Figure 3.13: Hot-wire measurement planes (Plane Z = 0, Plane Z = 23 mm).

The normalized velocity u/U_∞ profile along the centerline of the un-fined and unheated plate is shown in Fig. 14. The thickness of the boundary layer, δ, defined as the vertical distance from the surface of the plate to the location where the local velocity reaches 99% of the freestream value is tabulated in Table 3.1. From the similarity solution, the velocity profile for a turbulent boundary layer can be expressed as [43]

$$\frac{u}{U_\infty} = \left(\frac{y}{\delta}\right)^{1/7} \qquad (8)$$

The comparison between velocity profile obtained from measurement and the one-seventh-power distribution is depicted in Fig. 3.14. It is clear that even in the absence of the fin, the wedge fixture (see Fig. 3.2) causes significant disturbances to the incoming flow, making it a highly turbulent one.

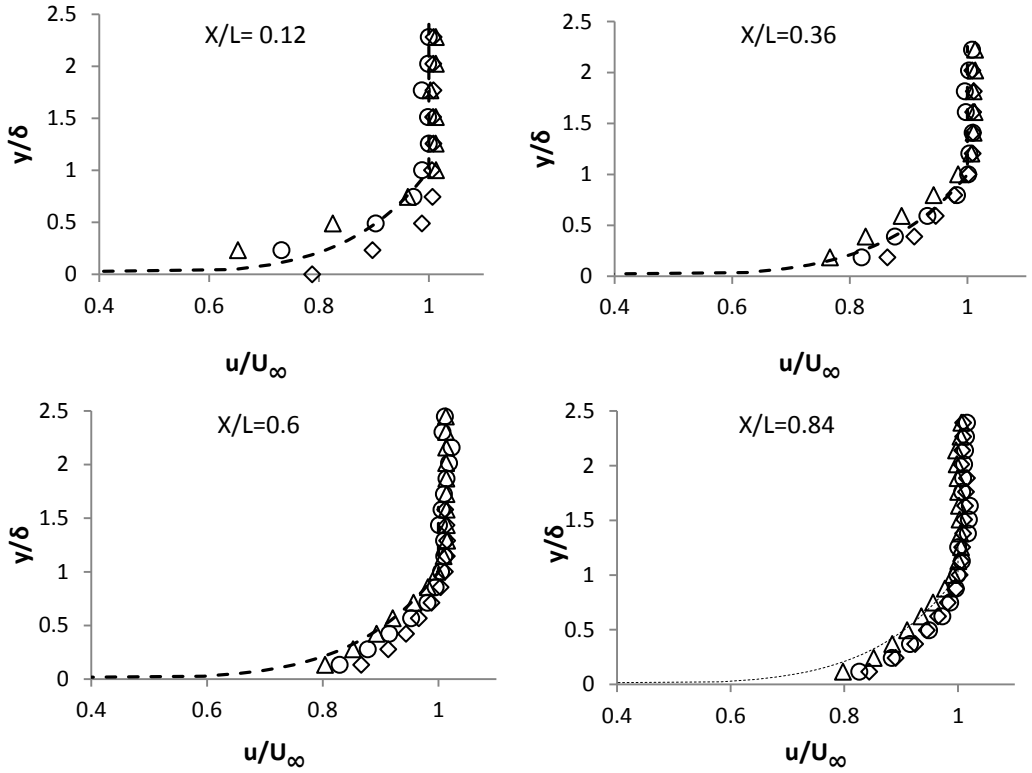

Figure 3.14: Velocity profile along the centerline of the unheated plate without turbulence generator. (◇, U_∞= 7.3 m/s; Δ, U_∞= 13.5 m/s; ○, U_∞= 20.9 m/s; ---, $1/7^{th}$ power velocity profile).

Table 3.1. Centerline boundary layer thickness for flow over the un-fined and unheated plate.

Streamwise location no.	1	2	3	4	5	6	7
X/L	0.12	0.24	0.36	0.48	0.60	0.72	0.84
δ (mm)	21.5	27.0	27.0	32.5	38.1	43.6	43.6

The turbulence intensities at different free stream velocities for four sections are portrayed in Fig. 3.15. With increasing distance from the leading edge to 24 centimeters downstream, the maximum turbulence intensity (at $y/\delta < 1$) decreases from about 15% to 8%. From 24 centimeters from the leading edge to the end of the plate, turbulence intensity reduces gradually to about 6%. As distance from the surface of the plate increases, the turbulence intensity decreases. At the outside of the boundary layer it approaches the free stream value. Also, it can be observed that for higher velocities the relative turbulence intensity is greater. The high turbulence intensity of the flow near the wall, along with the similarity of the shape of velocity profile with the one-seventh-power profile, confirms that the boundary layer near the wall is quite turbulent. Rigorously speaking, only wind tunnel flow with $Tu < 0.1\%$ can be considered to be laminar [44],

whereas the turbulence intensity of the incoming flow in the current wind tunnel is about 0.5%. The high turbulence intensity near the base of may be due to separation, recirculation, and reattachment features at the leading edge of the plate. Also, roughness of the surface and a gap between the leading part and the aluminum plate may serve as influential factors (see Fig. 3.2).

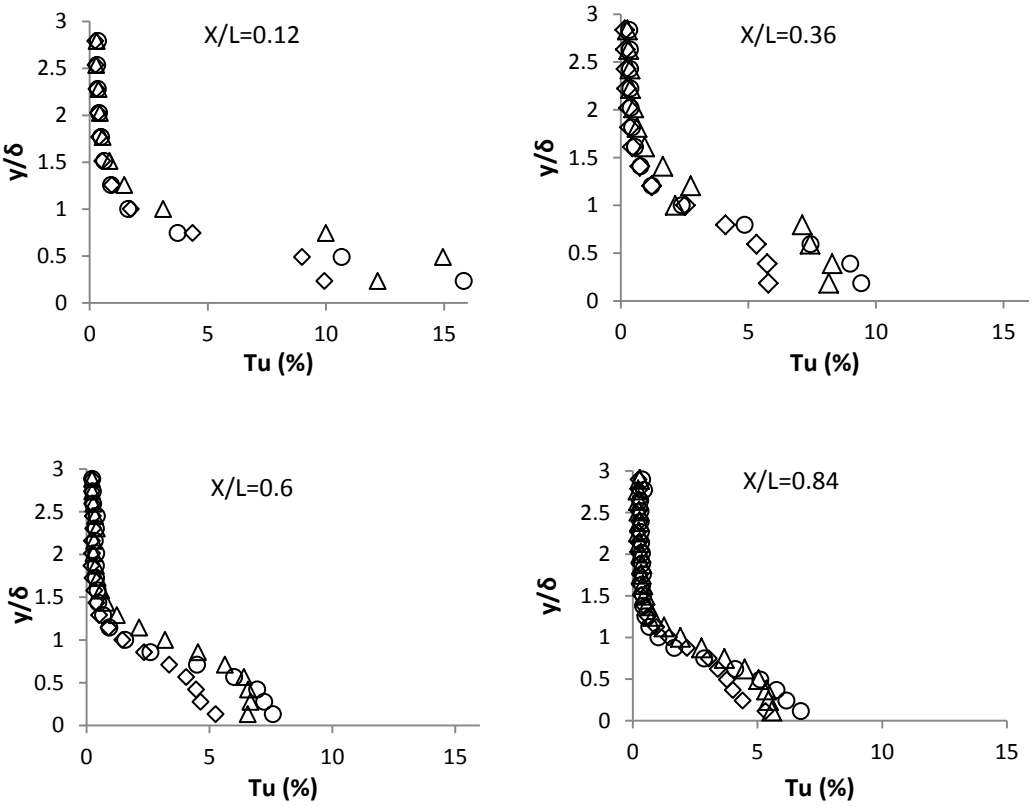

Figure 3.15: Turbulence intensity along the center line of plate in the absence of the turbulence generator. (◇, U_∞ = 7.3 m/s; Δ, U_∞ = 13.5 m/s; ○, U_∞ = 20.9 m/s).

Figure 3.13 illustrates the position of the hotwire and traversing path along the plate. Plane Z=0 represents the Z plane downstream of the most blocked part of the fin and Plane Z=23 mm is the most open Z plane. The corresponding velocity profiles along these two planes are depicted in Fig. 3.16. The effect of the opening / solidity on the velocity profile is clearly recognizable. The jets and wakes generated by the fin, and the shear imposed by the finite height (the upper edge) of the fin, result in some discontinuities in the velocity profile at X/L = 0.12. Farther downstream, however, the flow becomes homogenized with smooth velocity profiles. While the profiles downstream of Plane Z=0 are still differentiable from those downstream of Plane Z=23 mm at X/L= 0.36, 0.6 and 0.84, the differences at any particular cross section are relatively small. Knowing that these are the two extreme cases (Z planes), it may

concluded that the flow is relatively homogeneous (in the Z direction) beyond the wake-jet interaction regime.

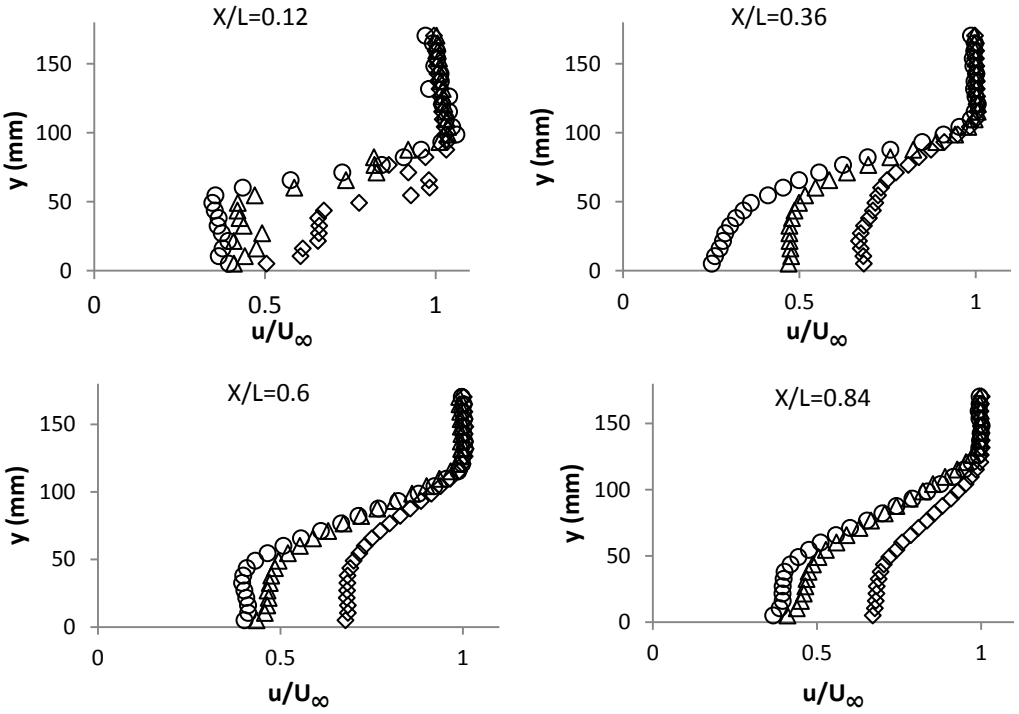

(a) Plane Z=0.

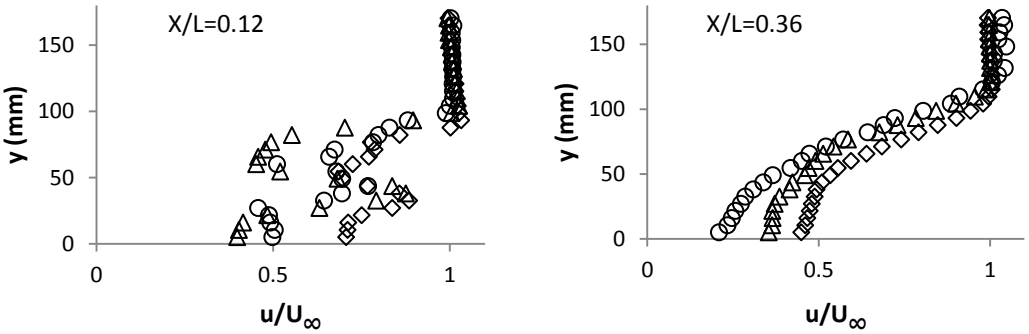

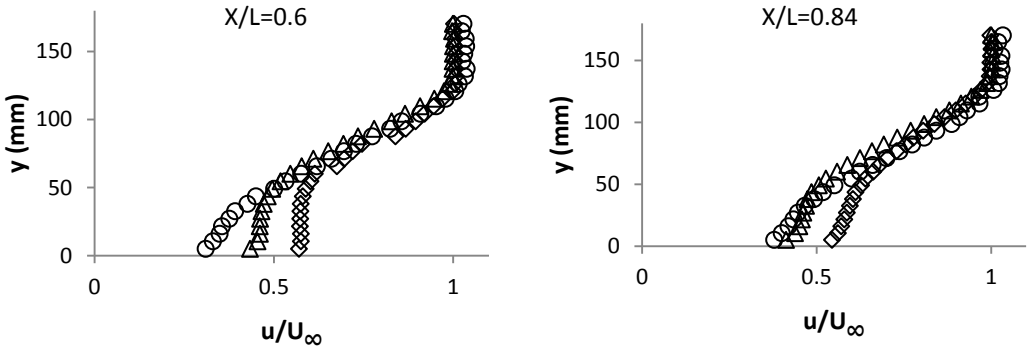

(b) Plane Z=23 mm.

Figure 3.16: Velocity profile behind the fin (a) Plane Z=0, (b) Plane Z=23 mm. (◇, U_∞= 7.3 m/s; Δ, U_∞= 13.5 m/s; ○, U_∞= 20.9 m/s).

It is clear from Fig. 3.16 that the fin has caused consistent velocity reduction of around 50% near the surface of the plate. The reduction also becomes more significant with increasing wind speed. More importantly, the local wind speed near the surface of the plate in the presence of the fin is notably lower than its counterpart in the absence of the fin as presented in Fig. 3.14. This is clearly a negative side effect of the current fin design, its relatively large blockage effect has limited convection heat transfer enhancement with respect to the no fin case to within a short distance downstream as shown in Fig. 3.12. To word it positively, in spite of the serious local wind speed reduction imposed by the blockage of the fin, there is still a positive convection heat transfer augmentation over the first portion of the surrogate solar panel. This net positive heat transfer enhancement is particularly encouraging when it can be seen that the non-ideal wedge-gap fixture (see Fig. 3.2) has resulted in significant turbulence generation in the baseline 'no fin' case (as compared to a laminar case).

To clearly depict the difference in the near surface wind speed, the difference between the dimensionless velocity in the absence of the fin with respect to that in the presence of the fin,

$$\Delta U^* = (\frac{u}{U_\infty})_{without\ fin} - (\frac{u}{U_\infty})_{with\ fin} \qquad (9)$$

has been plotted in Fig. 3.17. In this figure, ΔU_1^* and ΔU_2^* refer to this velocity difference at Z=0 and Z=23 mm, respectively. It is clear that the near-surface wind speed in the absence of the fin is always higher.

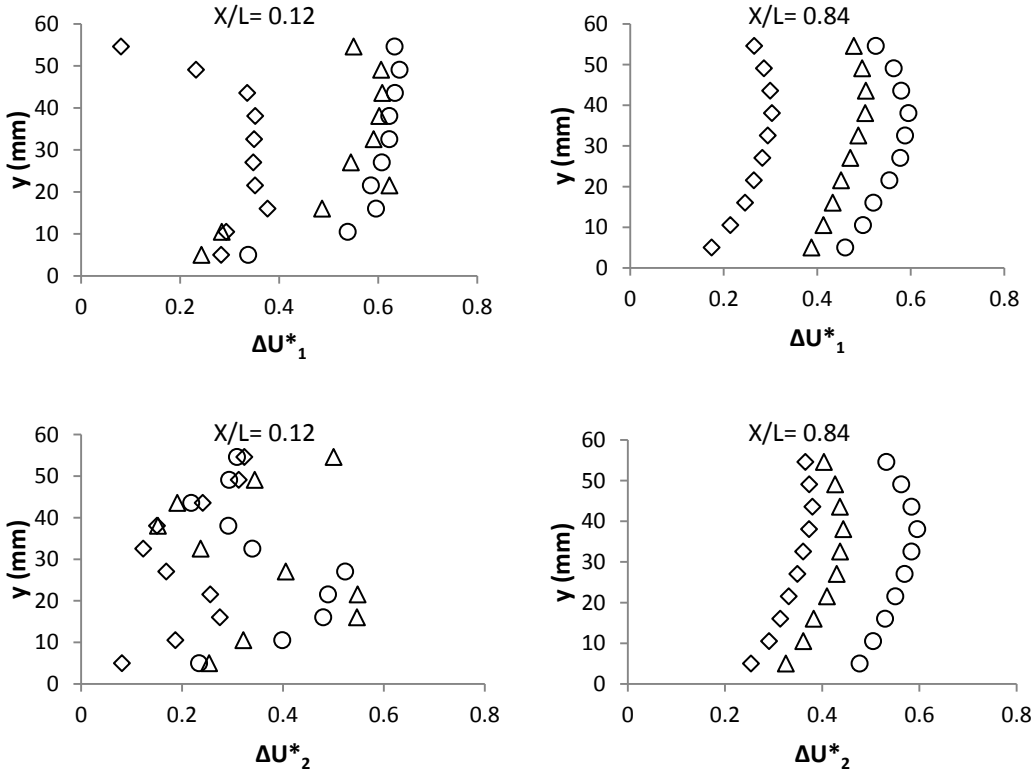

Figure 3.17: Local dimensionless velocity difference $((\frac{u}{U_\infty})_{without\ fin} - (\frac{u}{U_\infty})_{with\ fin})$. (◇, U_∞= 7.3 m/s; Δ△, U_∞= 13.5 m/s; ○, U_∞= 20.9 m/s).

To further reveal the underling physics behind the flow downstream of the fin, streamwise turbulence intensity is calculated. Figure 3.18 shows the turbulence intensity profile. Shortly downstream of the fin at X/L=0.12 (X=6 cm) the local turbulence intensity varies significantly, showing the inhomogeneous jet-wake interaction regime. Downstream of the hole where the velocity is high, the turbulence intensity is also high. As is the case with the velocity profile, this inhomogeneity quickly disappears farther downstream. It is clear that turbulence intensity increases with increasing wind speed. Most obviously, the turbulence intensity is highest around the shear layer downstream of the upper edge of the fin. It is unfortunate that this very intense turbulence region does not interject into the boundary layer in the current setup.

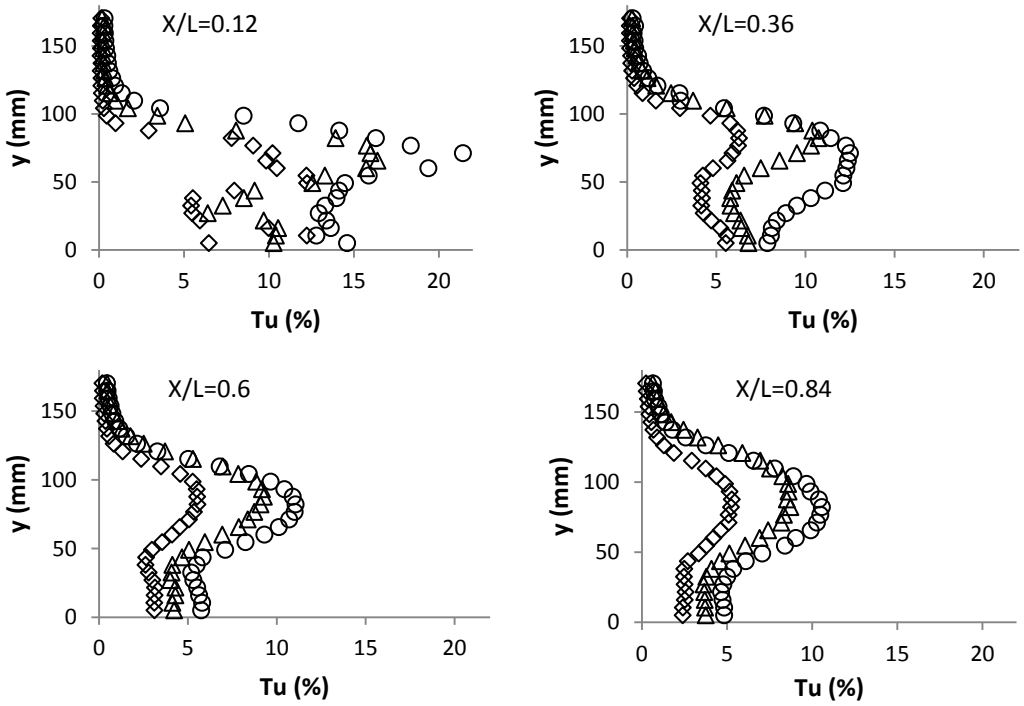

(a) Plane Z=0.

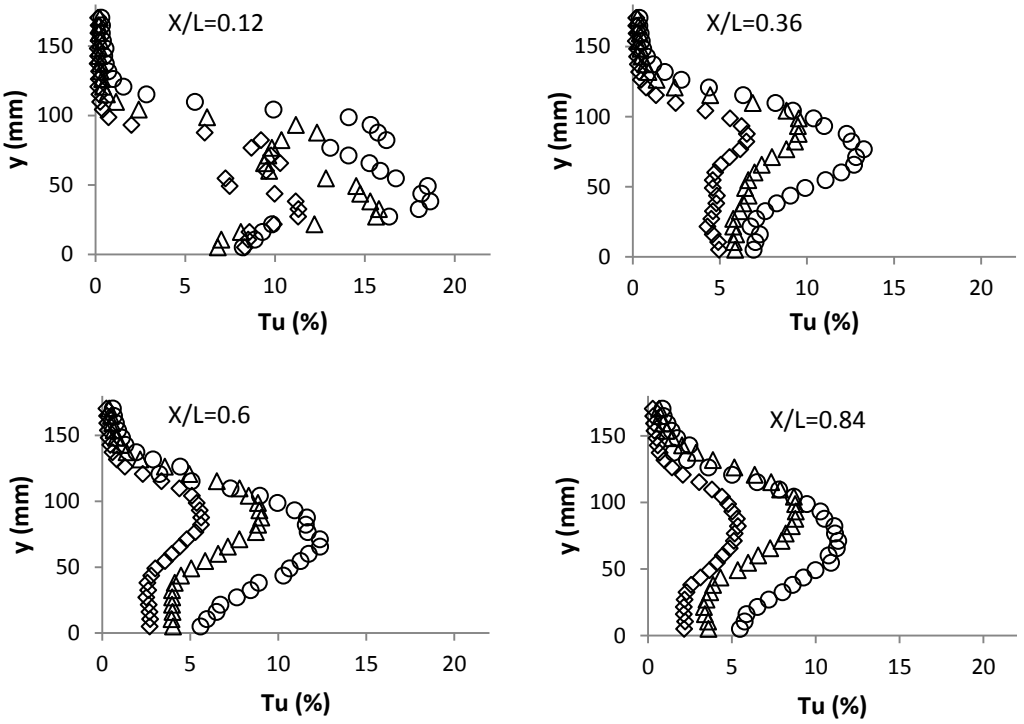

Figure 3.18: Turbulence intensity profile downstream of the fin (a) Plane Z=0, (b) Plane Z=23 mm. (◇, U_∞= 7.3 m/s; Δ, U_∞= 13.5 m/s; ○, U_∞= 20.9 m/s).

The change in the streamwise local turbulence intensity in the presence of the fin from that without the fin for Z=0 and Z=23 mm is illustrated in Fig. 19. In this figure, ΔTu_1 represents the difference of local turbulence intensity in Plane Z=0, and ΔTu_2 refers to difference in Plane Z=23 mm.

$$\Delta Tu = (Tu)_{without\ fin} - (Tu)_{with\ fin} \qquad (10)$$

Except in the region near the base, there is a clear enhancement in turbulence intensity in the absence of the fin, presumably due to the rough wedge with a gap fixture mentioned earlier. In other words, in spite of significant blockage effect, the fin still enhances the near wall (plate) turbulence beyond that rough wedge and a gap fixture does.

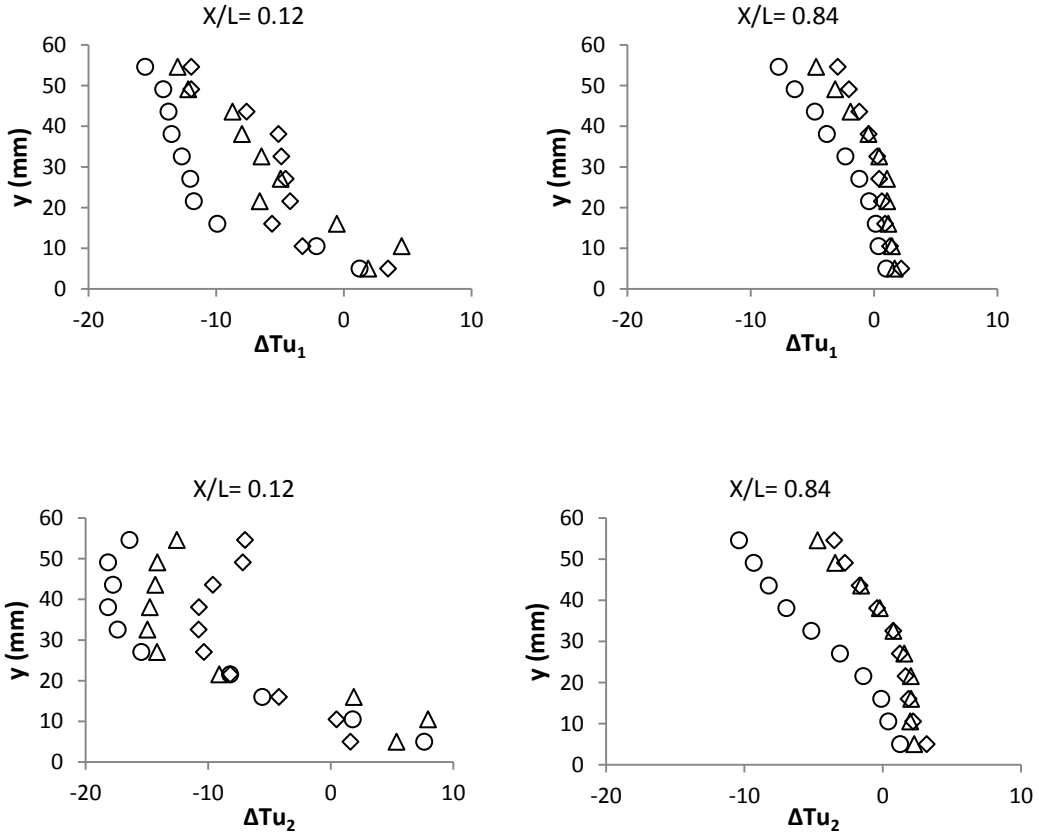

Figure 3.19: Local turbulence intensity difference ($(Tu)_{without\ fin} - (Tu)_{with\ fin}$). (◇, U_∞= 7.3 m/s; Δ, U_∞= 13.5 m/s; ○, U_∞= 20.9 m/s).

To examine the Nu-Re-Tu relationship at the fundamental level, the three non-dimensional parameters need to define such that they are functions of the local heat transfer coefficient, local near boundary wind speed and local near surface turbulence intensity, respectively. As such, the total length of the plate was chosen as the universal characteristic length. The local Nusselt number based on the local convection coefficient and total length of the plate in the streamwise direction can be written as follows

$$Nu_L = \frac{h_x L}{k} \tag{11}$$

The corresponding local Reynolds number can be defined as

$$Re_L = \frac{U^* L}{\vartheta} \tag{12}$$

where the average local velocity,

$$U^* = \frac{u_{(Y=5\ mm)} + u_{(Y=10.5\ mm)}}{2} \tag{13}$$

Accordingly, the local turbulence intensity,

$$Tu_L = \frac{Tu_{(Y=5\ mm)} + Tu_{(Y=10.5\ mm)}}{2} \tag{14}$$

The variation of this local Nusselt number along the streamwise direction (at X/L= 0.12, 0.36, 0.6 and 0.84) with local Reynolds number and local Turbulence intensity is presented in Fig. 3.20. The local Nusselt number, mean value of velocity and Tu for the finned case correspond to the mean value measured at Y=5 mm and Y=10.5 mm and averaged for Plane Z=0 and Plane Z=23 mm. The expected increase in Nusselt number with respect to Reynolds number and turbulence is clearly portrayed in Fig. 3.20, confirming the validity of the current results, for both un-finned and finned cases. More interestingly, the same amount of convective heat transfer enhancement per unit turbulence intensity can be achieved at a lower Reynolds number for the finned case of compared to the un-finned. This clearly suggests that the turbulence generated by the fin is more effective in augmenting heat transfer, provided the velocity (Reynolds number) reduction can be mitigated. The pronounced drop in Nusselt number with decreasing turbulence intensity at low levels of turbulence corresponds to the farthest downstream points considered. Turbulence has decayed to a rather low level at these relatively far stream locations. This and the thickened boundary layer, have presumably led to the significant lowering of Nusselt number.

(a) Without Fin

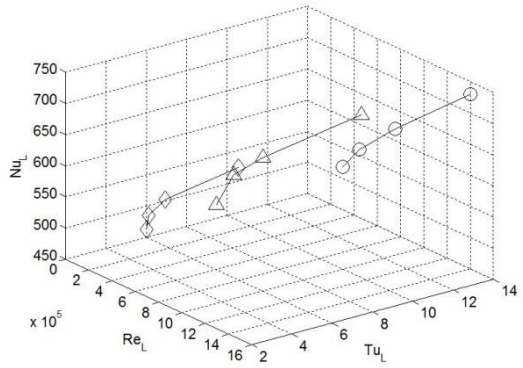

(b) With Fin

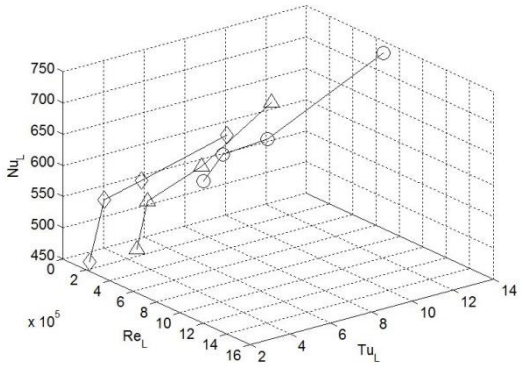

Figure 3.20: Relation between local Nusselt number, local Reynolds number and turbulence intensity. (◇, U_∞= 7.3 m/s; Δ, U_∞= 13.5 m/s; ○, U_∞= 20.9 m/s).

6. CONCLUDING REMARKS

In this study, an approach to passively cool a solar PV panel was initiated. A PV array was modeled using a heated aluminum flat plate placed in a wind tunnel. Temperature distribution and heat flux along the centerline of the plate with and without a turbulence generator (fin) were measured. The results showed that with the turbulence generator placed at the leading edge, the local surface temperature can only be lowered within a short span downstream of the turbulence generator. The finned local Nusselt number farther downstream is less than that of the corresponding un-finned one. This was found to be primarily due to the significant blockage imposed by the current fin, resulting in local wind speeds of approximately half the free stream velocity. Moreover, the non-ideal wedge with a gap fixture was found to seriously enhance the near-boundary layer flow turbulence, resulting in a highly turbulent boundary layer flow over the flat plate even in the absence of the fin. In terms of per unit turbulence intensity, the fin generated flow turbulence is found to be superior to the un-finned one. The key challenge in bettering the current fin design depends on reducing the blockage effect.

ACKNOWLEDGEMENTS

This work was made possible by Natural Sciences and Engineering Research Council of Canada. This is a project cosponsored by Ontario Centres of Excellence and Essex Energy Corporation.

REFERENCES

[1] Luque A., Hegedus S. 2nd Ed, Handbook of Photovoltaic Science and Engineering, Wiley, 2011.

[2] Ito M., Kato K., Komoto K., Kichimi T., Kurokawa K., A comparative study on cost and life-cycle analysis for 100 MW very large-scale PV (VLS-PV) systems in deserts using m-Si, a-Si, CdTe, and CIS modules. Progress in Photovoltaics: Research and Applications 16: 17–30, 2008.

[3] Shockley W., Queisser H. J., Detailed Balance Limit of Efficiency of p-n Junction Solar Cells, Journal of Applied Physics, 32 , 510-519, 1961.

[4] National Renewable Energy, Best Research Cell Efficiencies, http://www.nrel.gov/ncpv/images/efficiency_chart.jpg, Accessed on December 18, 2013.

[5] Top 10 World's Most Efficient Solar PV Mono-Crystalline Cells, http://www.solarplaza.com/top10-monocrystalline-cell-efficiency/#Sunpower, Accessed on April 18, 2013.

[6] Micheli L, Sarmah N, Luo X, Reddy K.S., Mallick K, Opportunities and challenges in micro- and nano-technologies for concentrating photovoltaic cooling: A review, Renewable and Sustainable Energy Reviews, 20: 595-610, 2013.

[7] Kumar R., Rosen M.A., Performance evaluation of a double pass PV/T solar air heater with and without fins, Applied Thermal Engineering 31: 1402-1410, 2011.

[8] Han X, Wang Y, Zh L. The performance and long-term stability of silicon concentrator solar cells immersed in dielectric liquids. Energy Conversion and Management; 66:189–98, 2013.

[9] Boer KW., Cadmium sulfide enhances solar cell efficiency. Energy Conversion and Management; 52(1):426–30, 2011.

[10] Tiwari A, Sodha MS. Parametric study of various configurations of hybrid PV/ thermal air collector: experimental validation of theoretical model. Solar Energy Material and Solar Cells; 91:17–28, 2007.

[11] Tonui JK, Tripanagnostopoulos Y. Performance improvement of PV/T solar collectors with natural air flow operation. Solar Energy; 82:1–12, 2008.

[12] Huang BJ, Liu TH, Hung WC, Sun FS. Performance evaluation of solar photovoltaic/thermal systems. Solar Energy; 70:443–8, 2001.

[13] Kalogirou SA, Tripanagnostopoulos Y. Hybrid PV/T solar systems for domestic hot water and electricity production. Energy Conversion and Management; 47:3368–82, 2006.

[14] Chow TT, He W, Ji J. Hybrid photovoltaic-thermosyphon water heating system for residential application. Solar Energy; 80:298–306, 2006.

[15] Ji J, Pei G, Chow TT, Liu K, He H, Lu J, et al. Experimental study of photovoltaic solar assisted heat pump system. Solar Energy; 82:43–52, 2008.

[16] Zhao X, Zhang X, Riffat SB, Su X. Theoretical investigation of a novel PV/e roof module for heat pump operation. Energy Conversion and Management; 52:603–14, 2011.
[17] Tang X, Zhao Y, Quan Z. The experimental research of using novel flat-plate heat pipe for solar cells cooling. In: Proceeding of the Chinese thermal engineering physics of heat and mass transfer conference; 22: 239–41, 2009.
[18] Zhang X., Zhao X., Smith S., Xu J., Yu X., Review of R&D progress and practical application of the solar photovoltaic/thermal (PV/T) technologies, Renewable and Sustainable Energy Reviews; 16: 599– 617, 2012.
[19] Zondag H.A. Flat-plate PV-thermal collectors and systems: a review, Renewable Sustainable Energy Review; 12: 891–895, 2008.
[20] Chow T.T. Photovoltaic/thermal hybrid solar technology: a review, Applied Energy; 87: 365–379, 2010.
[21] Krauter S. Increased electrical yield via water flow over the front of photovoltaic panels. Solar Energy Material and Solar Cells; 82:131–7, 2004.
[22] Royne A, Dey CJ. Design of a jet impingement cooling device for densely packed PV cells under high concentration. Solar Energy; 81:1014–24, 2007.
[23] Tonui J.K., Tripanagnostopoulos Y. Air-cooled PV/T solar collectors with low cost performance improvements, Solar Energy; 81 (4): 498–511, 2007.
[24] Bambrook S.M., Sproul A.B. Maximising the energy output of a PVT air system, Solar Energy; 86 (6): 1857–1871, 2012.
[25] Kim D., Bhattarai S., Oh J., Kim D-H. Simulation and Model Validation of the Surface Cooling System for Improving the Power of a Photovoltaic Module, Trans. ASME J. of Solar Energy Engineering; 133(4): 041012, 2011.
[26] Rahou M., Othman M. Y., Mat S., Ibrahim A. Performance Study of a Photovoltaic Thermal System With an Oscillatory Flow Design, Trans. ASME J. of Solar Energy Engineering; 136(1): 011012,2013.
[27] Tao H.G., Lee P.S., Hawlader M.N.A., An active cooling system for photovoltaic modules, Applied Energy; 90: 309–315, 2012.
[28] Liu L, Zhu L, Wang Y, Huang Q, Sun Y, Yin Z. Heat dissipation performance of silicon solar cells by direct dielectric liquid immersion under intensified illuminations. Solar Energy; 85:922–30, 2011.
[29] Skoplaki E., Palyvos J.A. On the temperature dependence of photovoltaic module electrical performance: a review of efficiency/power correlations, Solar Energy; 83: 614–624, 2009.
[30] Beccali M., Finocchiaro P., Nocke B., Energy and economic assessment of desiccant cooling systems coupled with single glazed air and hybrid PV/thermal solar collectors for applications in hot and humid climate, Solar Energy; 83: 1828–1846, 2009.
[31] Karava P., Jubayer C.M, Savory E., Li S. Effect of incident flow conditions on convective heat transfer from the inclined windward roof of a low-rise building with application to photovoltaic-thermal systems, Wind Engineering and Industrial Aerodynamics;104-106: 428-438, 2012.
[32] Bambara J., Experimental study of a facade-integrated photovoltaic/thermal system with unglazed transpired collector. M.Sc. Thesis, Department of Building, Civil and Environmental Engineering, Concordia University, Montreal, Canada, 2012.

[33] Sparrow E.M., Ramsey J.W., Mass E.A. Effect of finite width on heat transfer and fluid flow about an inclined rectangular plate, Trans. ASME J. Heat Transfer; 101: 199–204, 1979.
[34] Wang X.A., An experimental study of mixed, forced, and free convection heat transfer from a horizontal flat plate to air, Trans. ASME J. Heat Transfer; 104: 139–144, 1982.
[35] Francey J.L., Papaioannou J. Wind-related heat losses of a flat-plate collector, Solar Energy; 35: 15–19, 1985.
[36] Ito N., Kimura K., Oka J. A field experiment study on the convective heat transfer coefficient on exterior surface of a building, ASHRAE Trans. 78: 184–191, 1972.
[37] Sharples S., Full-scale measurements of convective energy losses from exterior building surfaces, Building and Environment; 19: 31–39, 1984.
[38] Loveday D.L., Taki A.H. Convective heat transfer coefficients at a plane surface on a full-scale building facade, Int. J. Heat Mass Transfer; 39 (8): 1729–1742, 1996.
[39] Clear R.D., Gartland L., Winkelmann F.C. An empirical correlation for the outside convective air-film coefficient for horizontal roofs, Energy and Building; 35:797–811, 2003.
[40] Hagishima A., Tanimoto J. Field measurements for estimating the convective heat transfer coefficient at building surfaces, Building and Environment; 38 (7): 873–881, 2003.
[41] Palyvos J.A, Survey of wind convection coefficient correlations for building envelope energy systems' modeling: a review, Applied Thermal Engineering; 28: 801–808, 2008.
[42] Cengel Y., 2nd Heat Transfer: A Practical Approach, McGraw-Hill Higher Education, 2003.
[43] Gad-el-hak M., Flow Control: Passive, Active and Reactive Flow Management, Cambridge University Press, London, 2000.
[44] Van Ingen L., The e^N method for transition prediction, Historical review of work at TU Delft, in: 38th AIAA Fluid Dynamics Conference and Exhibit, Seattle, Washington, AIAA paper 2008-3830, 2008.

CHAPTER 4

EFFECT OF A TRANSVERSE GROOVE ON COOLING OF A SURROGATE PHOTOVOLTAIC PANEL

ASME 2014 International Mechanical Engineering Congress & Exposition, IMECE 2014,November 14-20, 2014, Montreal, Canada, IMECE2014-37698

I.Arianmehr[*]
Turbulence & Energy Lab, Centre for Engineering Innovation
University of Windsor, Windsor, Ontario, Canada

D. S-K. Ting

Turbulence & Energy Lab, Centre for Engineering Innovation
University of Windsor, Windsor, Ontario, Canada

S. Ray
Essex Energy Corporation

Oldcastle, Ontario, Canada

1. ABSTRACT

Solar PV (photovoltaic) is a rapidly advancing renewable energy technology which converts sunlight directly into electricity. One of the significant performance challenges of many of the current commercial PV technologies is the reduction in its conversion efficiency with increasing PV panel temperature, which is closely associated with the increase in solar intensity and the ambient temperature where the technology is operating. In order to more effectively capture the available energy when the sun is most intense, significant efforts have been invested in active and passive cooling research over the last few years. While integrated cooling systems can lead to the highest total efficiencies, they are usually neither the most feasible nor the most cost effective solution. This work examines the effect of transverse square groove to manipulate the prevailing wind turbulence to enhance convective heat transfer over a heated plate in a wind tunnel.

NOMENCLATURE

h_x	local heat transfer coefficient ($\mathrm{W/m^2{}^\circ C}$)
k	thermal conductivity ($\mathrm{W/m^\circ C}$)

[*] Corresponding Author: iman.arianmehr@gmail.com.

L	total length of plate in streamwise direction (500 mm)
N	number of sample points in hotwire measurements (1000000)
Nu_x	local Nusselt number, based on h_x and streamwise distance from leading edge of plate, $Nu_x = h_x X/K$
q_x	local convection heat transfer(W/m^2)
T_f	film temperature (℃)
T_s	surface temperature (℃)
T_∞	free stream temperature (℃)
Tu	turbulence intensity, $Tu = \frac{u_{rms}}{U_\infty}$
u_i	instantaneous velocity (m/s)
u_{rms}	root-mean-square of the velocity fluctuation (m/s)
U_∞	free stream velocity (m/s)
$\overline{U}$	time averaged velocity (m/s)
X	streamwise distance from the leading edge (cm)
Y	vertical position from the surface (mm)
ΔT	temperature difference ($\Delta T = T_{grooved} - T_{w=0}$), (℃)

Greek Symbols

δ	boundary layer thickness (mm)

2. INTRODUCTION

Renewable energies can play a vital role in satisfying increasing demands for energy. Among them, solar energy is considered as one of the most promising sources of energy, since it offers safe, clean and abundant energy [1]. The application of PV (photovoltaic) cells for capturing the sun's radiation and converting it into direct current electricity is growing rapidly. The energy payback time for modern PV cells is estimated to be between 1 and 4 years [2]. Therefore, with a life expectancy of approximately 30 years for a typical PV cell, electricity can be generated profitably. Currently, the efficiency of the best non-concentrator mono crystalline silicon cells with dimensions of 2 cm × 2 cm in laboratory conditions is about 25% [3]. The world's highest modules have a demonstrated efficiency of approximately 23%, while the world record efficiency of concentrator multi-junction cells with four solar subcells is 44.7% [4]. Modern commercial crystalline silicon PV cells have an efficiency of less than 22.5% [5]. Thus, only a fraction of the incident solar energy is converted into electricity. The majority of absorbed sunlight is converted to heat, which increases the cells temperature. This can

lead to decreasing performance of the PV cells [6,7]. Also, high temperature can lead to irreversible damage, such as degradation due to thermal stresses, can lead to premature structural and conversion system failure [8,9]. Therefore, removing the waste heat from PV modules can improve their performance and mitigate premature aging.

The effect of a flowing film of water on the surface of a PV cell by placing a series of nozzles at the top of the module has been investigated by Krauter [10], where cell temperature reduction up to 22°C was observed. Also, the film of water decreased the reflection of sunlight by 2-3.6% and cleaned the surface of the module. The feasibility of impinging jet cooling for a highly dense array of PV array was investigated by Royne and Dey [11]. The characteristic of impinging jets is the non-uniform distribution of heat transfer coefficient, which was shown to be ineffective in improving the performance of PV cells. Also, it was concluded that the impinging liquid jet is more effective for scattering the generated heat from densely packed photovoltaic cells. A novel cooling method for PV cells under concentrated radiation was adduced by Liu et al [12]. They proposed increasing heat transfer from both front and back of the solar panel by directly immersing the cells in dimethyl-silicon oil, which is a dielectric liquid. The light source was a long-arc xenon lamp. The results showed the temperature distribution of module was almost uniform, with a maximum temperature difference of 3°C. Rahou et al. [13] studied the performance of integrated photovoltaic thermal roofing with an oscillatory flow design. Tao et al. [14] experimentally and numerically showed that by employing fin(s) in a duct flow and fabricating the duct at the back of the PV module, the electrical efficiency of a PV cell can increase from 8.6 to 12.5%.

Wind-induced convection heat transfer has been evaluated by many researchers. The effect of incident flow condition on forced convective heat transfer from integrated PVT systems on an inclined roof has been studied by Karava et al. [15]. Bambarda [16] investigated the efficiency of a corrugated, unglazed, transpired solar collector photovoltaic system.

A solution for cooling PV panels should be simple in order for it to be practical and versatile. Based on this mindset, we focus on passive cooling. Many PV panels come with a rigid rectangular frame, and thus, we look at the possibility of a small indentation in the form of a groove to perturb the incoming wind for enhancing passive convective cooling in this study. Although the effect of a transverse groove on a turbulent boundary layer has been studied for many years, it is not fully understood. Due to the different groove shapes with a range of various sizes, a wide range of results have been reported. The response of a turbulent boundary layer to three different shaped transverse grooves was studied by Sutardi and Ching [17]. They found that for higher free stream velocity the effect of a groove is more significant in increasing velocity just downstream of the groove, and that the most pronounced effect on turbulence intensity is caused by a square groove. In another study, they investigated the effect of three different sized square grooves on the turbulence boundary layer [18]. A general increase in turbulence intensity immediately downstream of the groove was disseminated in their study.

With infinite possible shapes and sizes, a general consensus on the definite quantitative effects of specific grooves on different flow conditions is still far from being achieved. The consequential influences on heat transfer downstream of a groove in external flow are more uncertain yet. Nonetheless, the qualitative enhancement in the

presence of grooves is quite clear, and thus, the investigation of heat transfer augmentation in ducts or channels by employing a rib, groove, or rib groove is extensive. In other words, the use of grooves as turbulence promoters is a common technique to enhance the heat transfer rate [19].

The current study examines the effect of a groove on the flow and heat transfer over a surrogate PV panel. Specifically, the width of the rectangular groove were varied to deduce its quantitative influence on the resulting convective heat transfer enhancement ability.

3. EXPERIMENTAL DETAILS

The experiments were carried out in a closed-loop horizontal wind tunnel with a 1.8 m long test section. The width and height of cross section are 0.76 m and 0.76 m. The experimental setup is depicted in Fig. 4.1. The maximum achievable mean velocity in the middle of empty test section is approximately 30 m/s. The background turbulence intensity level is less than 0.5% in the empty working section. The solar panel was surrogated by an aluminum flat plate with a dimension of 500 mm by 337 mm. The flat plate was equipped with a 457 mm × 304 mm silicon rubber heater that was connected to a DC power supplier to heat the plate. The surface temperature was monitored by 15 T-type thermocouples which were secured by adhesive pads at the back of the aluminum plate. The distance between two consecutive rows of thermocouple is 3 cm. A carbon fiber insulator and a particle board were applied underneath the heater to reduce heat loss from the back of the plate. The dimensions of the flat plate and arrangement of the thermocouples are depicted in Fig. 4.2.

In order to investigate the effect of a single groove on the characteristics of the flow and convective heat transfer, a bended U-shaped plate was attached at the leading edge of the flat plate; see Fig. 4.2. The U-shaped plate was bolted to the back of the particle board through five elongated holes, allowing easy groove width adjustments. The distance of the rectangular groove was 50 mm from the leading edge of the plate. In this study the widths of the grooves were 5 mm, 10 mm and 20 mm and the height of the rectangular groove was fixed at 5 mm.

A Dantec constant temperature anemometer (CTA) module 90C10 with a Dantec Type 55P15 one dimensional straight probe was used to quantify the air velocity and turbulence intensity. The platinum-plated tungsten wire sensor had a 5 μm diameter with a 1.25 mm active length. The analog voltage signals were first low-passed at 30 kHz using an analog filter to avoid aliasing, before being sampled at 80 kHz over 12.5 s (Sample Number = 1,000,000) through a 12 bit PCI-6071E National Instrument data acquisition card.

At the beginning of the experiment, a Pitot-static tube connected to a digital monometer (Dwyer series 475 mark II) was used to set the free-stream velocity to the desirable value. The measurement was conducted through a hole on the side wall of the wind tunnel test section. The local heat flux was measured by a heat transfer sensor manufactured by Hukseflux, (model PU-11) with overall diameter of 25 mm, sensitive dimension area of 10 × 10 mm, and an accuracy of ±5%.

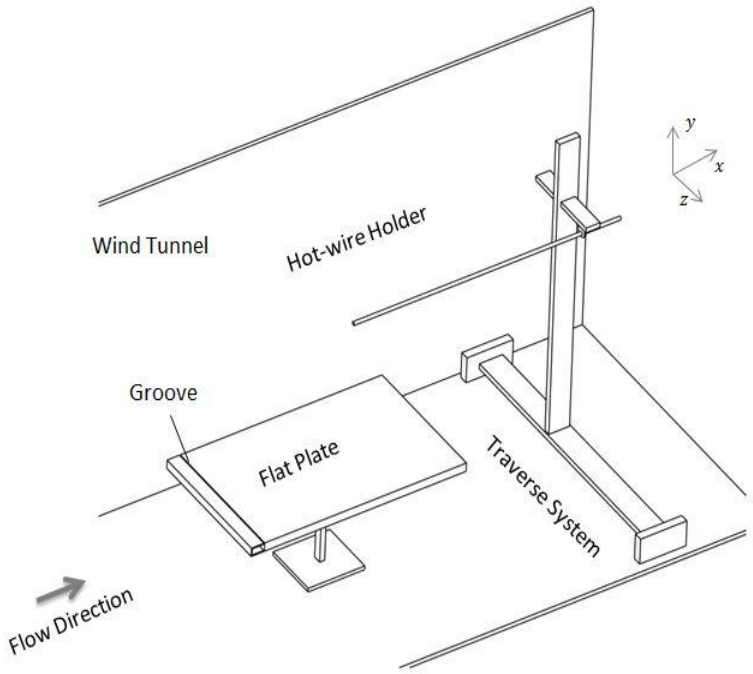

Figure 4.1: Schematic of experiment layout

Table 4.1. Centerline boundary layer thickness for flow over the unheated plate

Streamwise location no.	1	2	3	4	5	6
X/L	0.06	0.24	0.36	0.54	0.66	0.84
δ (mm)	32.5	49.1	60.1	65.6	76.3	87.6

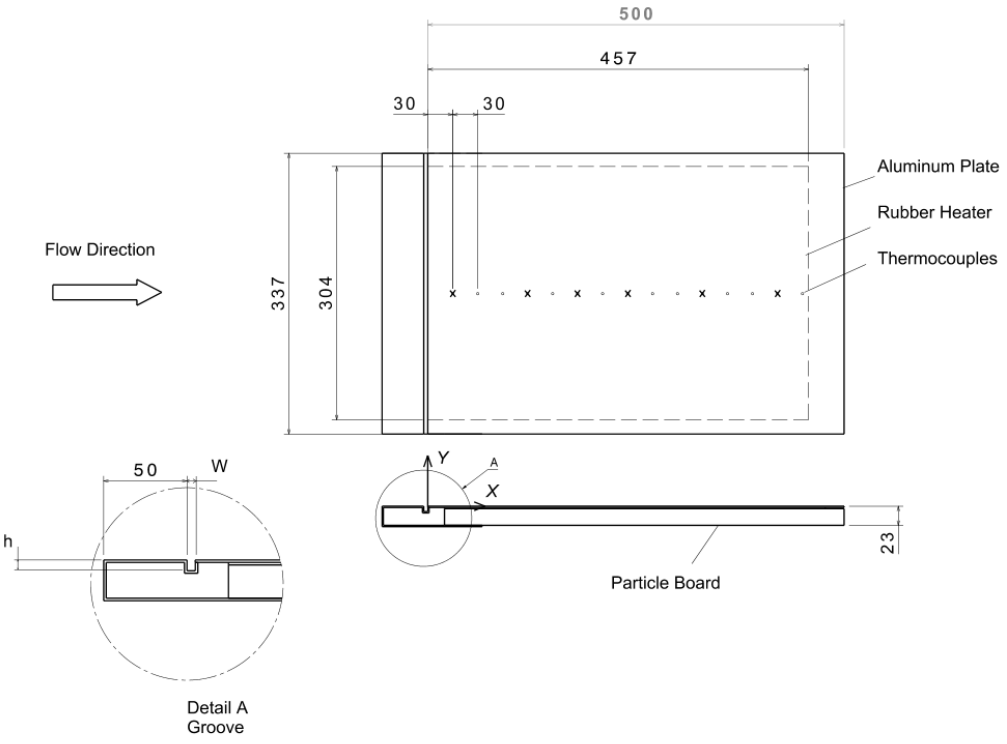

Figure 4.2: Configuration of the flat plate (dimensions are in mm)

4. RESULTS AND DISCUSSION

4.1. FLOW CHARACTRISTICS

A mean velocity measurement has been carried out at six streamwise sections along the centerline of the plate. The location of the sections in the X-Z plane are shown as crosses in Fig. 4.2. The non-dimensionalized distance of these sections from the leading edge of the groove in the streamwise direction have been summarized in Table 4.1, where the length of the aluminum plate *L* = 500 mm. The distance of the first section from the edge of the groove is 30 mm. The experiments were performed for freestream velocities of 6.5, 9.0, 12.5, and 16.0 m/s. At each cross-section, measurements were performed at thirty one points in the direction normal to the plate with a distance of 5.5 mm between two consecutive points. Due to space limitation, only results at the first, second, fourth, and sixth streamwise cross-sections are presented; the results at the third and fifth cross-sections fall between their corresponding neighbors. The normalized velocity u/U_∞ profile along the centerline of the plate for three different sizes of the

groove (W =0, 5, 10 and 20 mm) is portrayed in Fig. 4.3. The thickness of the boundary layer, δ, is defined as the vertical distance from the surface of the plate to the location where the local velocity reaches 99% of the freestream value. Table 4.1 shows the thickness of the boundary layer for flow over the plate without groove (W=0). As illustrated in Fig. 4.3, the effect of the groove (width) on velocity profile is not obvious. Only for higher velocities, U_∞=12.5 m/s and 16 m/s, at X/L=0.24, is the effect of the groove width easily discernible. There is an increase in u/U_∞ for all grooved cases compared to the W=0 case. More importantly, the near surface velocity seems to be increased with increasing groove size (width).

The laminar boundary layer velocity profile for a two-dimensional, incompressible, viscous flow over a flat plate can be predicted by nonlinear third-order Blasius equation [20]. From the similarity solution, the turbulent velocity profile can be approximated by the one-seventh power law [20]

$$\frac{u}{U_\infty} = \left(\frac{y}{\delta}\right)^{1/7} \qquad (1)$$

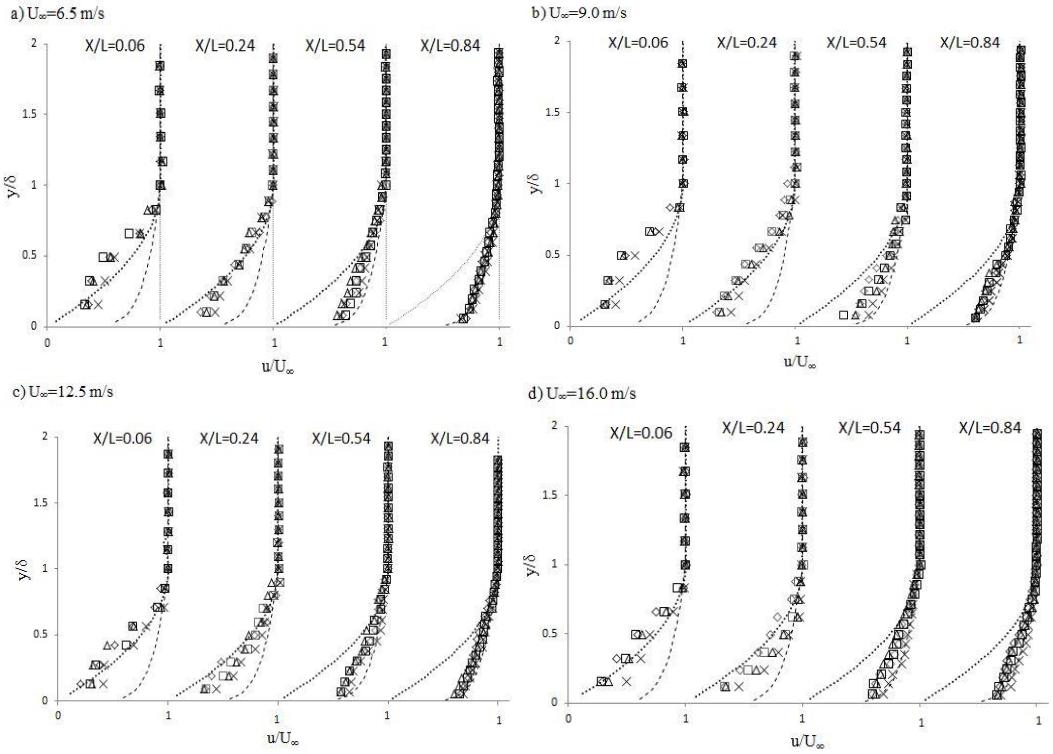

Figure 4.3. Velocity profile along the centerline of the unheated plate, (◇, W=0; □, W=5 mm; Δ, W=10 mm; ×, W=20 mm; … Blasius Profile; ---, 1/7th power velocity profile)

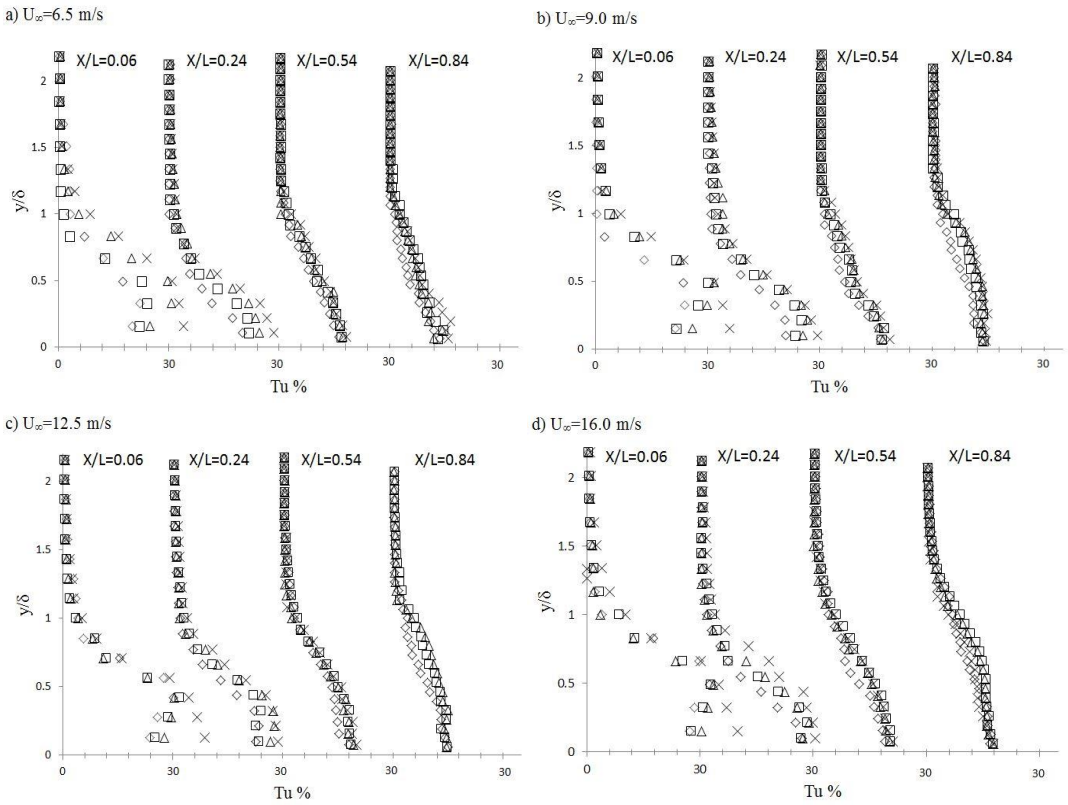

Figure 4.4. Turbulence intensity profile along the centerline of the unheated plate (◇, W=0; □, W=5 mm; Δ, W=10 mm; ×, W=20 mm)

For interest, the velocity profile along the plate for three cases has been compared to the Blasius and 1/7th power law velocity profiles in Fig. 4.3. It is clear that the velocity profiles, except those at the first and second streamwise locations due to the blunt leading edge, fall roughly between Blasius and the 1/7th velocity profile. The comparison between velocity profiles obtained from measurement and the one-seventh-power and Blasius distribution reveals that the current velocity profile is a highly nonconventional turbulent one, due to the blunt leading edge.

The velocity was measured as a series of discrete points, u_i. The mean velocity, $\overline{U}$, is defined as the time average of instantaneous measured velocity at each location. Turbulent fluctuation is defined as the difference between the instantaneous velocity and time averaged velocity.

The root-mean-square velocity is derived from

$$u_{rms} = \sqrt{\sum_{i=1}^{N} \frac{(u_i - \overline{U})^2}{N-1}} \qquad (2)$$

where sample size N=1×10^6. The relative turbulence intensity is

$$Tu = \frac{u_{rms}}{U_\infty} \times 100\% \qquad (3)$$

where U_∞ is the free stream velocity.

The turbulence intensities of different free stream velocities in the span wise (vertical) direction for four sections are depicted in Fig. 4a to 4d. Downstream of the groove, the maximum turbulence intensity in the boundary layer (at $y/\delta < 1$) decreases from about 33% to 15%. As the vertical distance from the surface of the plate increases, the turbulence intensity decreases and at the edge of the boundary layer it approaches the free stream value. Outside the boundary layer the turbulence intensity remains roughly constant in all cases. The high turbulence intensity of the flow near the wall, along with the similarity of the shape of the velocity profile to the one-seventh-power profile, confirms that the boundary layer near the wall is quite turbulent. Furthermore, only wind tunnel flow with $Tu < 0.1\%$ can be considered to be laminar [21], while the turbulence intensity of the incoming flow in the empty test section of the current wind tunnel is about 0.5%.

Comparison of the streamwise turbulence intensity profiles downstream of the groove are illustrated in Fig. 4.4. In the first and second streamwise locations, the effect of the groove size (width) on increasing turbulence intensity is discernible. The effect of the 20 mm groove in these locations is more pronounced compared to smaller grooves. Also, the turbulence intensity profile at the first streamwise location (X/L=0.06) for the 20 mm groove is different than for the other groove widths and the peak value is observed near the plate. The maximum turbulence intensity of the 20 mm groove at X/L=0.06 is higher than the peak value of the other cases. This seems to be consistent over the range of freestream velocities considered. As y/δ increases, the turbulence intensity profiles for all three groove sizes (W=5, 10, 20 mm) relax back to the values of the W=0 case.

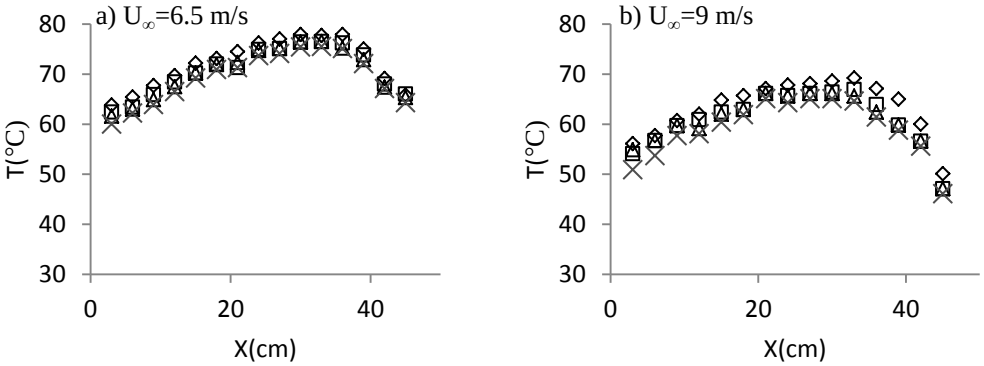

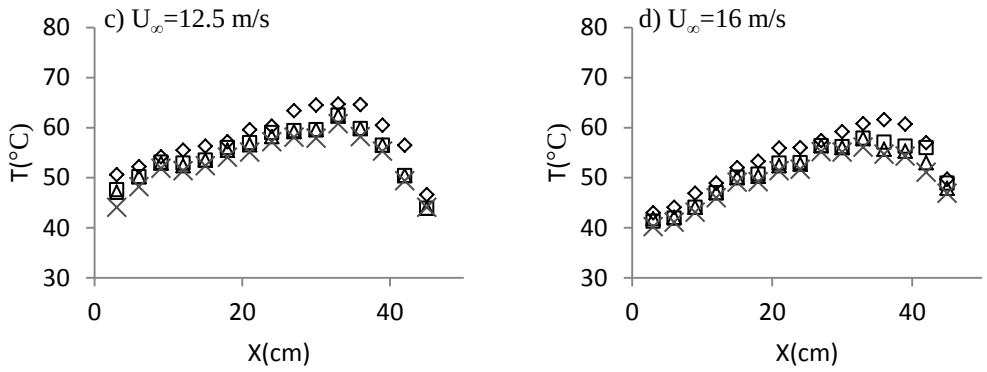

Figure 4.5: Variation of surface temperature along the centerline of the plate (◇,W=0; □, W=5 mm; Δ, W=10 mm; ×, W=20 mm)

4.2. HEAT TRANSFER ANALYSIS

The effects of the rectangular groove on temperature distribution and heat transfer of the heated plate were examined by opening the surface 50 mm downstream of the leading edge with a gap of 5, 10 and 20 mm. These results are cast with respect to those obtained with W=0. After turning the heater and the wind tunnel on, it took approximately two hours for the system to reach equilibrium. The temperature and heat flux were measured five times in a 15 minute interval, and the local temperature and heat flux along the plate were determined by the mean value at each point. The center region of the plate is least affected by any side edge effects, and hence, it was chosen for observation.

The mean temperature with an uncertainty of ±1°C along the centerline of the plate is outlined in Fig. 4.5. It can be seen that with increasing distance from the leading edge, the surface temperature rises, this may be partly due to the thickening of the boundary layer and the accumulation of thermal energy. Toward the end of the heated plate, the surface temperature decreases, presumably due to the trailing edge effect and the fact that the heater does not cover the last part of the plate (recall Fig. 4.2). This qualitative trend appears unchanged with variation in wind speed over the studied range. The overall (absolute) temperature, however, decreases with increasing wind speed as depicted in Figs. 4.5a to 4.5d. This is primarily due to the increased convection with increasing wind, for a fixed heat input. For all four wind speed cases considered, we see that increasing the gap width seems to promote the local heat transfer rate (i.e., lowers the surface temperature). In order to have a closer look at the effect of the groove, the temperature difference of the grooved scenario with respect to its ungrooved counterpart

$$\Delta T = T_{Grooved} - T_{W=0} \qquad (4)$$

has been depicted in Fig. 4.6. The effect of the groove on decreasing the temperature of the plate is clear. Also, there is an apparent effect of groove size in decreasing the temperature of the plate. The 20 mm groove has the most significant effect on temperature reduction.

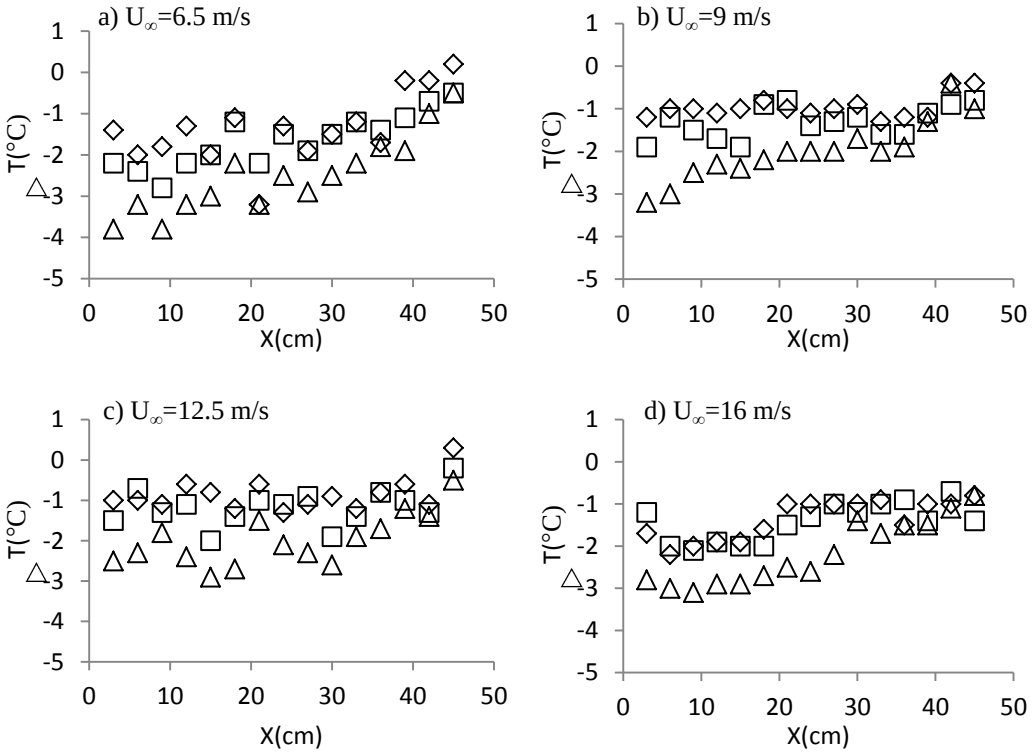

Figure 4.6: Local temperature difference along the centerline of the heated plate (◇,W=0; □, W=5 mm; Δ, W=10 mm; ×, W=20 mm)

The heat transfer coefficient can be determined from Newton's law of cooling

$$q_x = h_x(T_s - T_\infty) \qquad (5)$$

The local Nusselt number is thus

$$Nu_x = \frac{h_x X}{k} \qquad (6)$$

where k (W/m℃) is the thermal conductivity of the air at the film temperature ($T_f = \frac{T_s+T_\infty}{2}$) [22].

The local heat transfer coefficient against distance downstream of the groove has been plotted in Fig. 4.7. It is clear that the heat transfer coefficient decreases with

distance X, which is primarily due to the thickening of the boundary layer. As expected, the heat transfer coefficient also increases with wind speed, which is clearly observed for all four groove sizes.

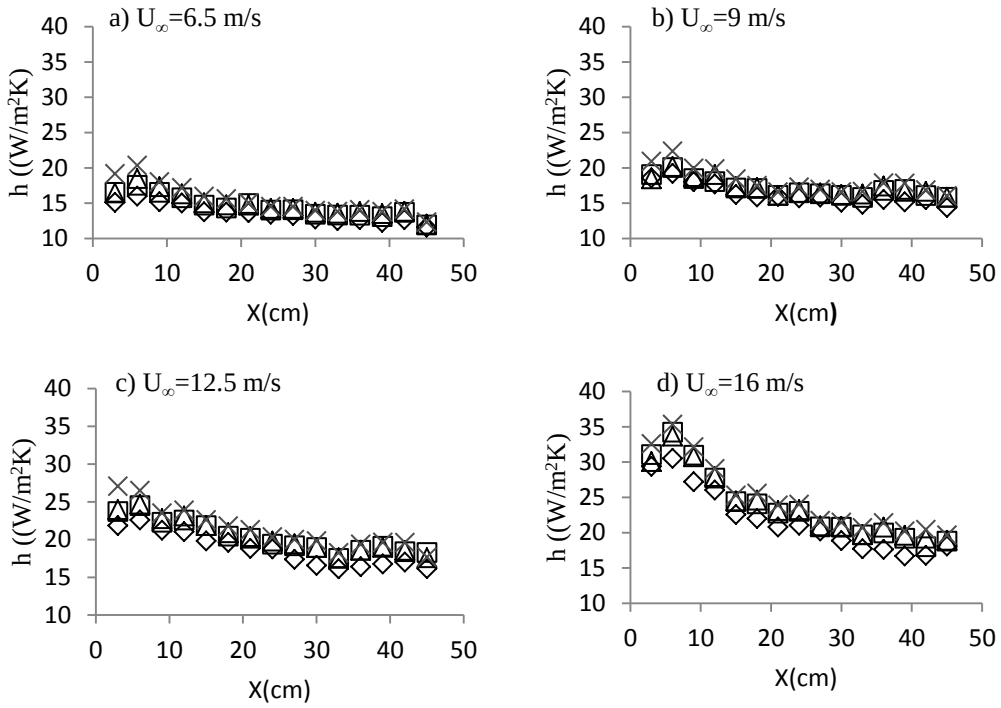

Figure 4.7: Variation of convection coefficient along the centerline of the heated plate (◇,W=0; □, W=5 mm; Δ, W=10 mm; ×, W=20 mm)

To better illustrate the effect of the different size (width) of grooves on the effectiveness of the local heat transfer, the local Nusselt number of the grooved cases (W= 5, 10, 20 mm) are normalized with respect to that without groove (W=0) in Fig. 4.8.

$$Normalized\ Nu_x = \frac{grooved\ Nusselt\ umber}{ungrooved\ Nusselt\ number} \quad (7)$$

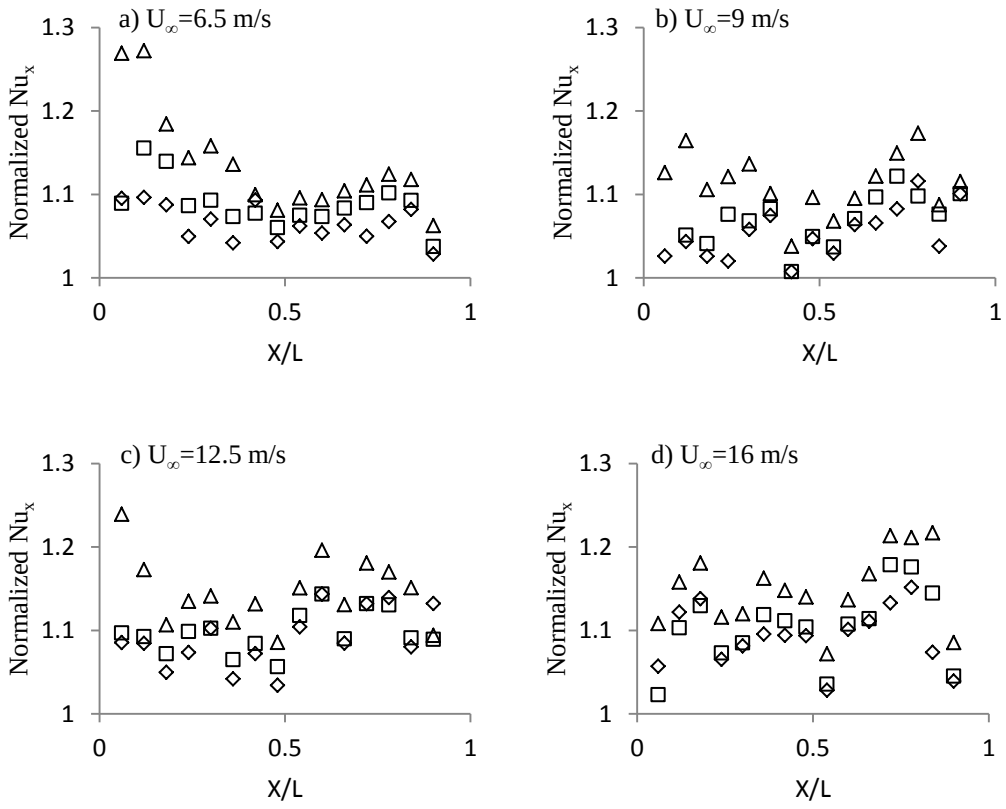

Figure 4.8: Normalized Nusselt number along the centerline of the plate (◇,W=5 mm; □, W=10 mm; Δ, W=20 mm)

The figure shows that the groove has a clear positive effect in enhancing the local Nusselt number downstream of the groove. The uncertainty associated with the normalized Nusselt number is approximately 5%. While a specific trend regarding the amount of enhancement with respect to the streamwise distance is not discernable, the enhancement itself is consistent and certain. Also consistent is the fact that the largest (20 mm) groove increases the local Nusselt number most significantly.

The average Nusselt number for the span of the heated surface under consideration can be deduced as [22]

$$\overline{Nu} = \frac{1}{L}\int_0^L Nu_x dx \qquad (8)$$

$$\overline{Nu} = \frac{1}{n}\sum_{i=1}^{n} Nu_x \qquad (9)$$

The values of these average Nusselt numbers for different groove size are summarized in Table 4.2. A quick comparison reveals that by increasing the size of groove the average Nusselt number increases.

Table 4.2. Mean Nusselt number for different groove size

$\overline{Nu}$	W=0	W=5 mm	W=10 mm	W=20 mm
U_∞=6.5 m/s	117.1	123.6	125.6	128.3
U_∞=9 m/s	140.8	142.7	144.5	146.4
U_∞=12.5 m/s	158.8	161.7	162.8	166.5
U_∞=16 m/s	175.9	185.1	184.7	188.1

5. CONCLUSION

In this study, an approach to passively cool a solar PV panel was undertaken. A PV panel was modeled using a heated aluminum flat plate placed in a wind tunnel. Characteristics of the flow, temperature distribution and heat flux along the centerline of the plate for three different sizes of groove (W=5, 10, 20 mm) were quantified and the results were compared with respect to the ungrooved case (W=0). The results showed the local surface temperature of the plate downstream of the groove can be lowered up to 4 °C. The heat transfer enhancement of the groove decreased with streamwise distance, but lasted until the end of the plate. The augmentation of convective heat transfer was found to increase with the size (width) of the groove, with the W=20 mm groove providing the greatest augmentation. Characteristics of the underlying flow reveal that the effect of these grooves on local velocity is subtle, where the near surface velocity is marginally increased with groove size (width). The augmentation in the near-surface turbulence with groove width is more discernible, especially just downstream of the groove. It is believed that the augmented near-surface flow turbulence along with the subtle increase in near-surface flow have led to the unambiguous heat transfer enhancement.

ACKNOWLEDGEMENTS

This work was made possible by Natural Sciences and Engineering Research Council of Canada. This is a project cosponsored by Ontario Centres of Excellence and Essex Energy Corporation.

REFERENCES

[1] Luque A., Hegedus S. 2nd Ed, Handbook of Photovoltaic Science and Engineering, Wiley, 2011.

[2] Ito M., Kato K., Komoto K., Kichimi T., Kurokawa K., A comparative study on cost and life-cycle analysis for 100 MW very large-scale PV (VLS-PV) systems in deserts using m-Si, a-Si, CdTe, and CIS modules. Progress in Photovoltaics: Research and Applications 16: 17–30, 2008.

[3] National Renewable Energy, Best Research Cell Efficiencies, http://www.nrel.gov/ncpv/images/efficiency_chart.jpg, Accessed on December 4, 2013.

[4] World Record Solar Cell with 44.7% Efficiency, http://www.soitec.com/en/news/press-releases/world-record-solar-cell-1373/.

[5] Top 10 World's Most Efficient Solar PV Mono-Crystalline Cells, http://www.solarplaza.com/top10-monocrystalline-cell-efficiency/#Sunpower, Accessed on April 18, 2013.

[6] Micheli L, Sarmah N, Luo X, Reddy K.S., Mallick K, Opportunities and challenges in micro- and nano-technologies for concentrating photovoltaic cooling: A review, Renewable and Sustainable Energy Reviews, 20: 595-610, 2013.

[7] Kumar R., Rosen M.A., Performance evaluation of a double pass PV/T solar air heater with and without fins, Applied Thermal Engineering 31: 1402-1410, 2011.

[8] Han X, Wang Y, Zh L. The performance and long-term stability of silicon concentrator solar cells immersed in dielectric liquids. Energy Conversion and Management; 66:189–98, 2013.

[9] Boer KW., Cadmium sulfide enhances solar cell efficiency. Energy Conversion and Management; 52(1):426–30, 2011.

[10] Krauter S. Increased electrical yield via water flow over the front of photovoltaic panels. Solar Energy Material and Solar Cells; 82:131–7, 2004.

[11] Royne A, Dey CJ. Design of a jet impingement cooling device for densely packed PV cells under high concentration. Solar Energy; 81:1014–24, 2007.

[12] Liu L, Zhu L, Wang Y, Huang Q, Sun Y, Yin Z. Heat dissipation performance of silicon solar cells by direct dielectric liquid immersion under intensified illuminations. Solar Energy; 85:922–30, 2011.

[13] Rahou M., Othman M. Y., Mat S., Ibrahim A. Performance Study of a Photovoltaic Thermal System With an Oscillatory Flow Design, Trans. ASME J. of Solar Energy Engineering; 136(1): 011012,2013.

[14] Tao H.G., Lee P.S., Hawlader M.N.A., An active cooling system for photovoltaic modules, Applied Energy; 90: 309–315, 2012.

[15] Karava P., Jubayer C.M, Savory E., Li S. Effect of incident flow conditions on convective heat transfer from the inclined windward roof of a low-rise building

with application to photovoltaic-thermal systems, Wind Engineering and Industrial Aerodynamics;104-106: 428-438, 2012.

[16] Bambara J., Experimental study of a facade-integrated photovoltaic/thermal system with unglazed transpired collector. M.Sc. Thesis, Department of Building, Civil and Environmental Engineering, Concordia University, Montreal, Canada, 2012.

[17] Choi K.S., Fujisawa N., Possibility of drag reduction using d-type roughness, Applied Scien- tific Research, 50: 315–324, 1993.

[18] Wahidi R., Chakroun W., Al-Fahed S., The behavior of the skin-friction coefficient of a turbulent boundary layer flow over a flat plate with differently configured transverse square grooves, Experimental Thermal and Fluid Science, 30: 141–152, 2005.

[19] Sutardi, Ching C.Y., Effect of different sized transverse square grooves on a turbulent boundary layer, Experiments in Fluids, 34: 261–274, 2003.

[20] Sutardi, Ching C.Y., The response of a turbulent boundary layer to different shaped transverse grooves, Experiments in Fluids, 35: 325–337, 2003.

[21] Gad-el-hak M., Flow Control: Passive, Active and Reactive Flow Management, Cambridge University Press, London, 2000.

[22] Van Ingen L., The e^N method for transition prediction, Historical review of work at TU Delft, in: 38th AIAA Fluid Dynamics Conference and Exhibit, Seattle, Washington, AIAA paper 2008-3830, 2008.

[23] Cengel Y., 2nd: Introduction to Thermodynamics and Heat Transfer, McGraw-Hill Higher Education, 2008.

CHAPTER 5

CONCLUSION AND RECOMMENDATIONS

This chapter presents a number of concluding remarks about the investigation that was undertaken to ascertain turbulence convective heat transfer for cooling the photovoltaic cells. Several recommendations for further research are subsequently outlined in the closing section of this thesis.

SUMMARY AND CONCLUSIONS

The effect of an orifice perforated plate (fin) for passively cooling a surrogate PV panel was studied in Chapters 2 and 3. A PV panel was modeled using a heated aluminum flat plate placed in a wind tunnel. Temperature distribution and heat flux along the centerline of the plate with and without a turbulence generator (orifice perforated plate) were measured. The results showed that with the perforated plate placed at the leading edge, the local surface temperature can only be lowered within a short span downstream of the turbulence generator. The finned local Nusselt number farther downstream is less than that of the corresponding un-finned one. The measurement of the flow characteristics revealed that in the presence of the fin, the local wind speed downstream of the fin near the wall only reaches up to half of the free stream velocity. This was found to be due to significant blockage imposed by the turbulence generator. Moreover, the gap between the wedge and plate promotes turbulent boundary layer for flow over the flat plate even in the absence of the fin.

In Chapter 4, the effect of a transverse groove with constant depth (5 mm) and variable width on cooling the modeled photovoltaic panel was studied. The results showed that the local surface temperature of the plate downstream of the groove can be lowered up to 4 °C just downstream of the groove. The effect of the grooves faded along the streamwise direction of the plate, but remained positive up to the end of the plate. The effect of 20 mm groove was more significant than smaller grooves. The effect of the grooves merges together as the flow approaches the end of the plate. Characteristics of the flow reveal that the effect of a 20 mm groove on turbulence intensity is more significant in the first downstream location.

Recommendations

This section provides some recommendations for future research.

- Experiments have been carried out for a particular perforated orifice plate. It would have been interesting to consider a different size of turbulence promoter.
- The background turbulence intensity of the freestream was constant at 0.5%. However the turbulence intensity of the wind in the field is higher than this value. The effect of passive cooling can be studied for different ranges of free stream turbulence intensities.
- In this study, the focus was on the flow parallel to the plate. Research should also be carried out to the effect of a turbulence generator for flow over an inclined plate.
- While in Chapter 4, the emphasis has been placed on the effect of the transverse groove, the use of different surface roughness should yield better results on the way a turbulent boundary layer responds to the surface. For instance, if there are combined with riblets, they might improve further turbulence cooling of the PV panel.
- In this study the PV panel is modeled by an aluminum flat plate. Since there are significant physical differences between our wind tunnel model and real PV panel, it is recommended to study efficiency of a photovoltaic panel by exposing it to a stable and uniform halogen light source.

APPENDICES

Appendix A

WAVELET ANALYSIS

In the Fourier theory, a signal can be expressed as the sum of an infinite series of sines and cosines. The Fourier transform consists of only frequency resolutions, but it does not have time resolution. It means that only presented frequencies in a signal can be determined. Wavelet transform is one of the solutions to overcome shortcoming of the Fourier transform [1]. Wavelet transform decomposes a signal into a set of functions. These functions are called wavelet [2]. Wavelet transforms provide a way for analyzing the waveforms, bounded both in frequency and duration [3]. Wavelet analysis has attracted much attention in signal processing.

Flow velocity over the un-finned flat plate was captured by hotwire anemometry with sampling frequency of 80 KHz and sampling number of 1000000. Consequently the sampling period is 12.5 s. The sampling signal for a point along at middle of the plate and with 15 cm height from the surface of the plate has been presented in Fig. 1. The original signal versus the number of sample has been depicted in Fig. 2.

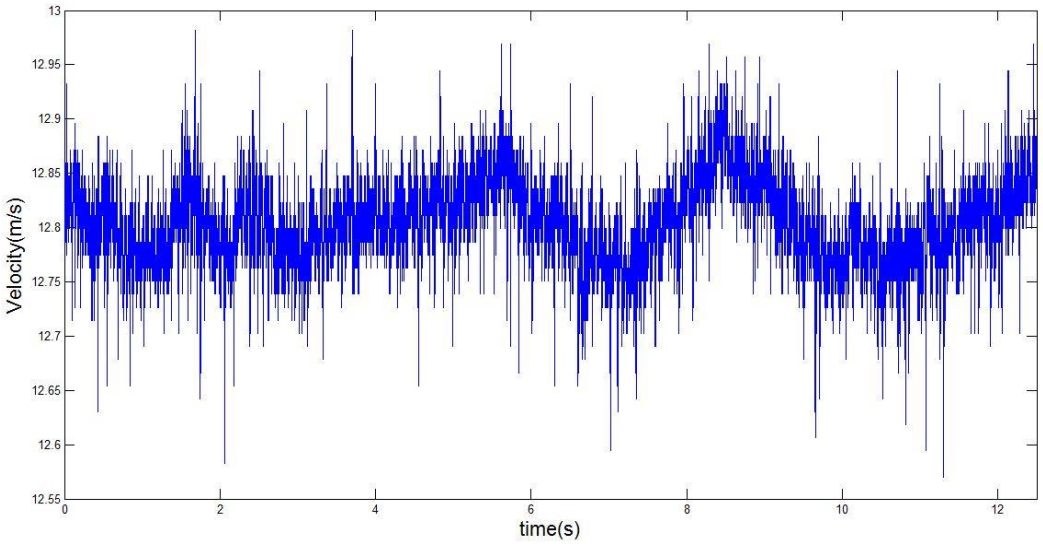

Figure A.1. Sampling Signal vs time

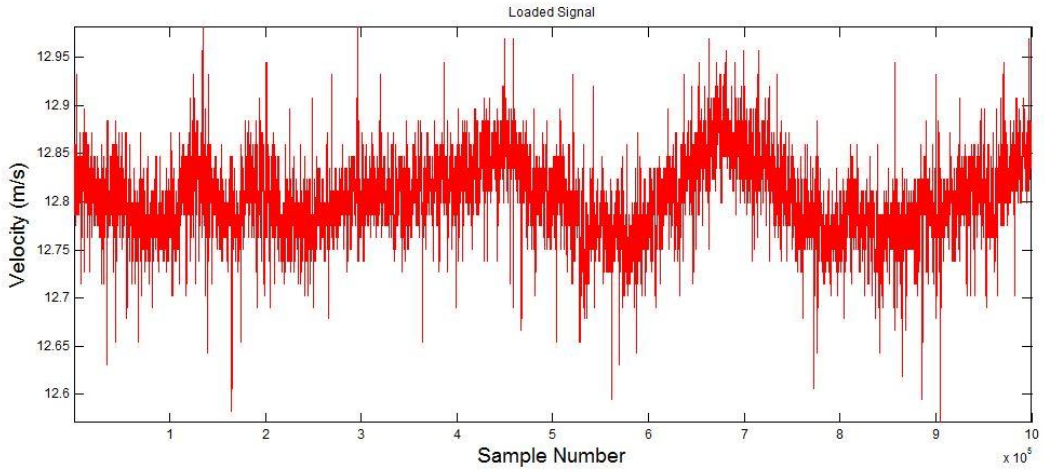

Figure A.2. Original signal versus sample number

In order to have the frequency content of this signal locally in time, wavelet analysis has been applied. For decomposition of this signal Daubechies function with vanishing moments of 7 and in the level of 10 has been utilized. This function is widely used in solving a board range of problem [4]. Vanishing moment in db7 means that wavelet coefficient for 7^{th} order polynomial will be zero. The mother signal based on decomposition at level 12 can be written as

$$S = d1 + d2 + \cdots + d12 + a12 \qquad (1)$$

where S is mother (origin) signal, d is detail signal and a is approximation signal. The wavelet tree, origin signal, and approximation signal at level 12 has been depicted in Fig. 3. The detail and approximation signal in each level has been illustrated in Fig. 4.

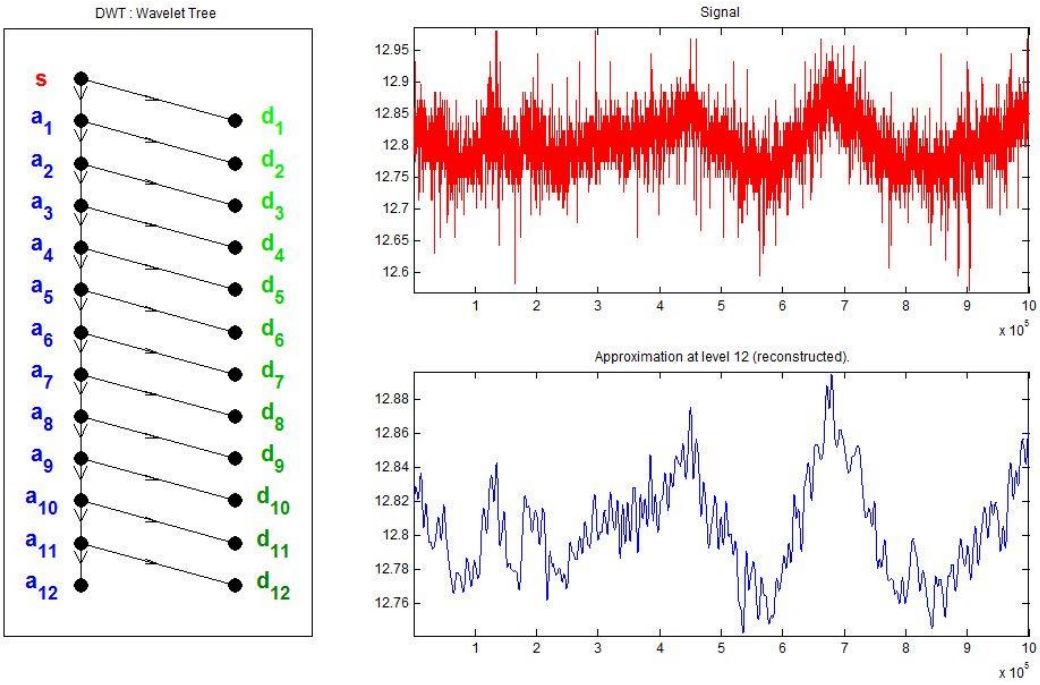

Figure A.3. The wavelet tree

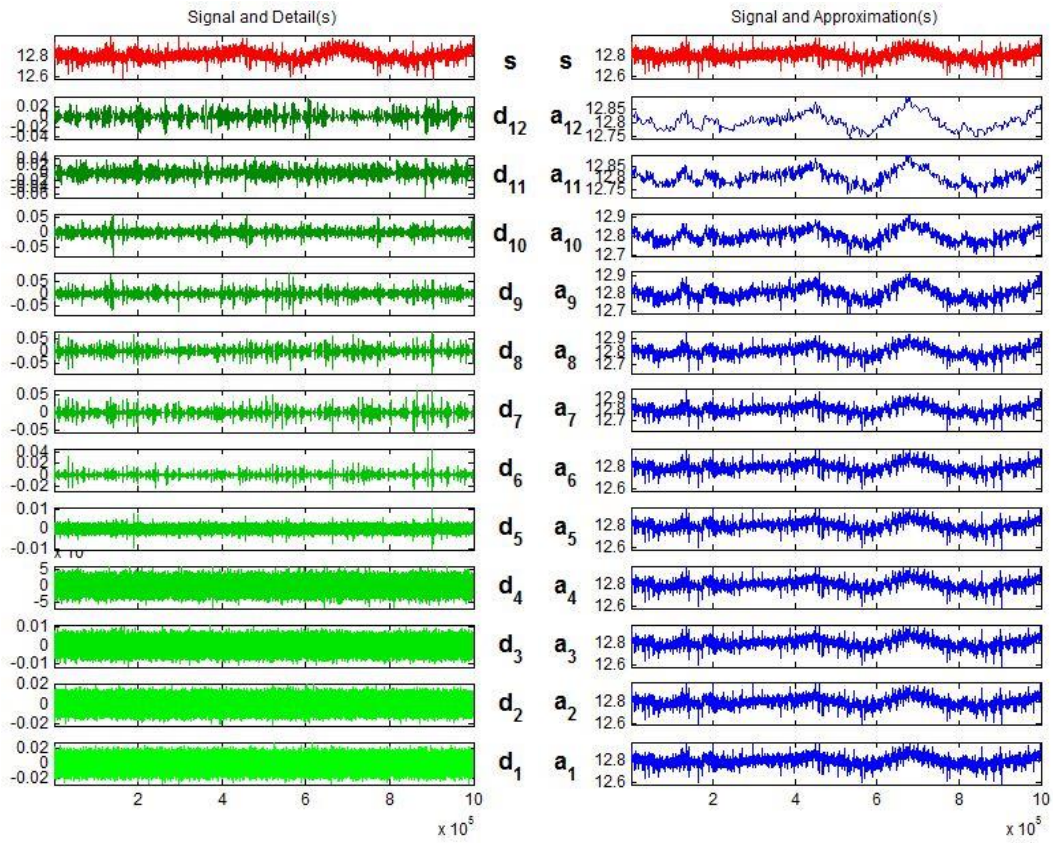

Figure A.4. Detail and approximation signal in each level

REFERENCES

[1] http://www.cs.unm.edu/~williams/cs530/arfgtw.pdf

[2] http://www.slideshare.net/piyush_11/discrete-wavelet-transform

[3] http://cseweb.ucsd.edu/~baden/Doc/wavelets/qiao_wavelet_intro.pdf

[4] http://en.wikipedia.org/wiki/Daubechies_wavelet

Appendix B

PERMISSIONS FOR PREVIOUSLY PUBLISHED WORKS

Chapter 2: Assisted Turbulence convective heat transfer for cooling the photovoltaic cells

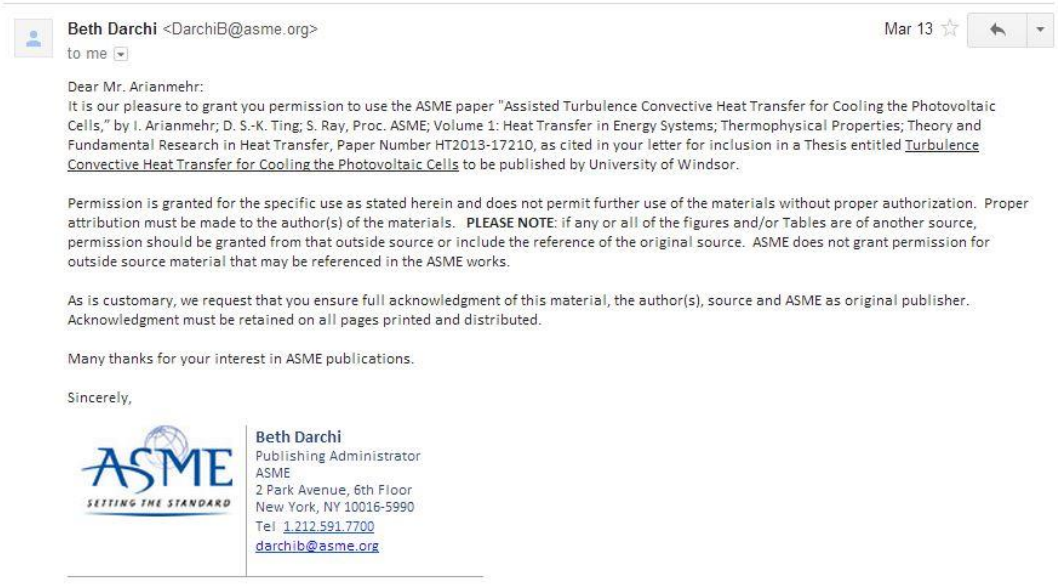

Beth Darchi <DarchiB@asme.org> Mar 13

to me

Dear Mr. Arianmehr:
It is our pleasure to grant you permission to use the ASME paper "Assisted Turbulence Convective Heat Transfer for Cooling the Photovoltaic Cells," by I. Arianmehr; D. S.-K. Ting; S. Ray, Proc. ASME; Volume 1: Heat Transfer in Energy Systems; Thermophysical Properties; Theory and Fundamental Research in Heat Transfer, Paper Number HT2013-17210, as cited in your letter for inclusion in a Thesis entitled Turbulence Convective Heat Transfer for Cooling the Photovoltaic Cells to be published by University of Windsor.

Permission is granted for the specific use as stated herein and does not permit further use of the materials without proper authorization. Proper attribution must be made to the author(s) of the materials. **PLEASE NOTE**: if any or all of the figures and/or Tables are of another source, permission should be granted from that outside source or include the reference of the original source. ASME does not grant permission for outside source material that may be referenced in the ASME works.

As is customary, we request that you ensure full acknowledgment of this material, the author(s), source and ASME as original publisher. Acknowledgment must be retained on all pages printed and distributed.

Many thanks for your interest in ASME publications.

Sincerely,

ASME SETTING THE STANDARD

Beth Darchi
Publishing Administrator
ASME
2 Park Avenue, 6th Floor
New York, NY 10016-5990
Tel 1.212.591.7700
darchib@asme.org

Chapter 3: Effect of a Transverse Groove on Cooling of a Surrogate Photovoltaic Panel

This article has not yet been submitted to the Journal of Solar Energy Engineering and therefore permissions cannot be obtained for the release of copyright. Upon submission of the article appropriate permissions are to be obtained in order to maintain the rights to publish this work.

Chapter 4: Convective Cooling of a Surrogate Photovoltaic Panel with a Transverse Groove

This article has not yet been submitted to the Journal of Solar Energy Engineering and therefore permissions cannot be obtained for the release of copyright. Upon submission of the article appropriate permissions are to be obtained in order to maintain the rights to publish this work.

VITA AUCTORIS

NAME:	Iman Arianmehr
PLACE OF BIRTH:	Rasht, IRAN
YEAR OF BIRTH:	1981
EDUCATION:	Iran University of Science and Technolgy, B.Sc., Tehran, Iran, 2006
	University of Mohaghegh Ardabili, M.Sc., Ardabil, Iran, 2009
	University of Windsor, M.Sc., Windsor, ON, Canada, 2014